nature metabolism

Letter

https://doi.org/10.1038/s42255-026-01485-0

Python metabolomics uncovers a conserved postprandial metabolite and gut–brain feeding pathway

Received: 5 June 2025

Accepted: 10 February 2026

Published online: 19 March 2026

Check for updates

Shuke Xiao[1,2,3,23], Mengjie Wang[4,22,23], Thomas G. Martin[5,6,23], Barry Scott[7], Xing Fang[4], Xinming Liu[4,22], Yongjie Yang[4,22], Sipei Fu[1,2,8], Steven D. Truong[9,10], Jack F. Gugel[5,6], Gregory L. Maas[5,6], Marcus P. Mullen[6,11], Jennifer Hampton Hill[5,6], Veronica L. Li[1,2], Andrew L. Markhard[1,2], Mingming Zhao[12,13], Wei Qi[8], Saranya C. Reghupaty[1,13,14], Meng Zhao[15], Jan Spaas[1,2], Wei Wei[16], Trine Moholdt[17,18], John A. Hawley[19], Christian T. Voldstedlund[20], Erik A. Richter[20], Xiaoke Chen[8], Katrin J. Svensson[1,13,14], Daniel Bernstein[12,13], Leslie A. Leinwand[5,6] ✉, Yong Xu[4,22] ✉ & Jonathan Z. Long[1,2,3,13,14,21] ✉

Most mammals consume small and frequent meals. By contrast, pythons are ambush predators that exhibit extreme feeding and fasting patterns and provide a unique model for uncovering molecular mediators of the postprandial response[1–3]. Using untargeted metabolomics, we show that circulating levels of the metabolite *para*-tyramine-O-sulphate (pTOS) are increased more than 1,000-fold in pythons after a single meal. In pythons, pTOS production occurs in a microbiome-dependent manner via sequential decarboxylation and sulphation of dietary tyrosine. In both pythons and mice, pTOS administration activates a neural population in the ventromedial hypothalamus (VMH). In mice, these VMH neurons are required for the anorexigenic effects of pTOS. Chronic administration of pTOS to diet-induced obese male mice suppresses food intake and body weight. pTOS is also present in human blood, where its levels are increased after a meal. Together, these data uncover a conserved postprandial anorexigenic metabolite that links nutrient intake to energy balance.

Organismal energy homeostasis is a highly dynamic process that is strongly influenced by nutrient availability. Nutrient consumption induces a postprandial phase marked by the release of neuroendocrine signals and hormones, such as insulin, which promote anabolism and nutrient storage. Conversely, in the fasted state, the release of other metabolic messengers, such as glucagon, induce a shift towards mobilization of internal energy reserves. To date, much of our understanding about the endocrine control of energy homeostasis during feeding or fasting comes from studies in mammals such as humans and rodents. While informative, mammals are nevertheless adapted to consuming small (<1–2% of body weight) and frequent (1–3 times per day) meals. This physiology places a fundamental limit on the degree to which fluctuations of energy states and postprandial physiological responses can occur.

By contrast, the Burmese python (*Python molurus bivittatus*) offers a striking example of an organism that demonstrates extreme feeding and fasting patterns, and postprandial physiology[1–3]. Burmese pythons are ambush predators that can fast for extended periods, sometimes up to 12–18 months. When they feed, they can consume prey equal to their own body weight in a single meal[1]. After such a meal, Burmese pythons

A full list of affiliations appears at the end of the paper. ✉e-mail: leslie.leinwand@colorado.edu; yongx@bcm.edu; jzlong@stanford.edu

display a remarkable array of postprandial responses, including more than 40-fold increase in energy expenditure, sustained tissue protein synthesis and more than 50% increase in the size of most organs[4–11]. Upon completion of digestion, many of these responses revert to levels close to that of the original fasted state[1,2,11–13], demonstrating that these snakes undergo an extreme and reversible postprandial responses with every meal. Beyond Burmese pythons, many other members of the Pythonidae family also exhibit sit-and-wait predatory lifestyles and extreme feeding and fasting patterns, including ball pythons (*Python regius*), African rock pythons (*Python sebae*) and reticulated pythons (*Malayopython reticulatus*)[11,14].

We hypothesized that the extreme feeding patterns and physiological responses of pythons would also be mirrored by equally extreme molecular responses. Therefore, the python could provide a unique opportunity to discover postprandial molecules that would otherwise be missed in more classical organisms, such as mammals, which have more limited fluctuations in their energy states and postprandial physiology. Such molecules would not only be most readily detectable in pythons but would also likely be potentially informative for mammalian physiology.

To date, only a limited number of previous efforts have sought to understand postprandially regulated molecules in such a physiologically extreme organism[4,15–17]. For instance, metabolomic studies revealed an increase in fatty acids and bile acids in postprandial python plasma[4], a mixture of which was shown to be sufficient to stimulate cardiac hypertrophy when administered to either pythons or mice[4]. However, these past studies have been relatively narrowly focused on a small set of predefined molecules. We reasoned that an unbiased metabolomic analysis of plasma from fasted and fed pythons might reveal unrecognized signalling molecules that have a critical role in the python postprandial response. Using untargeted metabolomics, we identified a metabolite, *para*-tyramine-O-sulphate (pTOS) as the most dramatically induced metabolite (>1,000-fold) in postprandial python plasma. Follow-up studies in both pythons and mammals show that pTOS functions as a conserved anorexigenic postprandial metabolite gut–brain signal.

Results

Metabolomics of postprandial python plasma

We used both targeted and untargeted metabolomics to identify circulating metabolites significantly altered by feeding in Burmese pythons. Pythons (approximately 2 years old and weighing 1.5–2.5 kg at the start of the study) were fed once every 28 days, with each meal amounting to approximately 25% of their body weight. Plasma samples were collected from fasted pythons and from pythons killed 3 days after feeding (Fig. 1a).

In the comparison between 3 days after feeding and fasted python plasma samples, our targeted metabolomics platform detected several metabolites that were increased by 4–20-fold postprandially. For instance, we observed an increase in many circulating amino acids, especially the non-essential amino acids glycine (20-fold) and proline (ninefold) (Extended Data Fig. 1a). Fumarate and malate were also increased by 4–8-fold (Extended Data Fig. 1b). Lastly, several species of very-long-chain fatty acids, such as lignoceric acid (C24:0), hexacosanoic acid (C26:0) and hexacosenoic acid (C26:1) were also increased by 4–6-fold (Extended Data Fig. 1c).

In our untargeted metabolomics platform, many more metabolites with even more dramatic increases after feeding were detected. Using a cut-off of a twofold change[5], we found 208 metabolite features significantly ($P_{adj} < 0.05$) increased, and 24 metabolites significantly decreased in plasma from 3 days after feeding versus fasted samples (Fig. 1b and Supplementary Table 1). The metabolite feature with the greatest fold increase after feeding (>1,000-fold) in python plasma was an unknown molecule with a mass-to-charge ratio (*m/z*) of 218.0487 in positive ionization mode ($P_{adj} = 2.1 \times 10^{-3}$; Fig. 1c). This exact mass enabled us to deduce a chemical formula for the parent ion of $C_8H_{11}NO_4S$. Tandem mass spectrometry (MS/MS) of this feature revealed two distinct fragment ions: one at *m/z* 201.0187, indicating the loss of an NH_3 group; and another at *m/z* 121.0634, corresponding to the neutral loss of a sulphate group (SO_3). This $C_8H_{11}NO_4S$ metabolite feature was also detectable in negative ionization mode with an *m/z* of 216.0331 (Extended Data Fig. 2a) and a loss of sulphate (−80) (Extended Data Fig. 2b) upon MS/MS fragmentation. Based on the parent chemical formula and fragmentation patterns, we surmised that this metabolite contained a primary amine, a phenolic sulphate group and two additional methylene groups. Therefore, we tentatively assigned the structure as pTOS (Fig. 1d). This structural assignment was confirmed when the endogenous plasma peak was compared to an authentic pTOS standard generated via chemical synthesis: the authentic standard matched both the fragmentation pattern (Fig. 1d and Extended Data Fig. 2b) and the retention time (Extended Data Fig. 2c) of the endogenous metabolite in both positive and negative ionization modes.

Quantitative analyses revealed that plasma pTOS concentrations increased from 20 ± 5 nM in the fasted state to 1.0 ± 0.1 µM at 1 day after feeding and peaked at 4.5 ± 0.6 µM at 3 days after feeding in Burmese pythons (Fig. 1e). To determine the generality of postprandial pTOS increases, we also measured plasma pTOS levels in ball pythons (*P. regius*), a species that diverged from Burmese pythons approximately 21 million years ago (Fig. 1f). In ball pythons, a similar postprandial rise in pTOS was observed: pTOS concentrations in the fasted state were 1.2 ± 0.6 nM, increased to 1.5 ± 0.4 µM by 1 day after feeding and peaked at 4.1 ± 1.2 µM at 3 days after feeding. In ball pythons, we collected a longer postprandial plasma time course and observed that pTOS levels drastically decreased to submicromolar levels at 6 days after feeding, and back to nanomolar range at 10 and 15 days after feeding (Fig. 1f). The time course is similar (peak at days 1–3) to that previously reported for metabolic rate changes after a meal in pythons[18].

pTOS levels and postprandial regulation in humans and mice

pTOS is a poorly studied metabolite. In humans, sporadic reports have detected pTOS in urine as a rapidly excreted molecule[19,20]. Its presence in circulation and postprandial regulation in humans had not been rigorously studied.

We first examined public metabolomic datasets where circulating metabolites were measured before and after a meal test in humans. We identified three study cohorts and a total of six meal tests where blood pTOS measurements were available. The first 'HuMet' study cohort consisted of 15 healthy male participants who were exposed to several physiological challenges, including three standardized liquid diet meals[21]. The first meal consisted of a recovery meal after a 36-h fast ('recovery standardized liquid diet'); under these conditions, pTOS levels increased by 2–8-fold (Fig. 1g). The other two meals also led to increases of pTOS by an average of ~1.5-fold and ~3-fold (Extended Data Fig. 3a,b). Interestingly, in the same study, pTOS levels also decreased over the initial 36-h fasting period (Fig. 1h). The second study cohort ('Moholdt') consisted of $n = 24$ healthy young men who followed either a habitual diet or brief high-fat diet (HFD) feeding[22]. In this study, circulating pTOS levels were measured either before breakfast or after dinner and exhibited an average approximate fivefold increase after dinner regardless of the diet (Extended Data Fig. 3c,d). One individual exhibited more than a 30-fold increase in pTOS levels. The third study cohort ('Agueusop') examined the metabolic changes before and 1 h after a standardized mixed meal in $n = 30$ individuals who were either healthy, prediabetic or with type 2 diabetes[23]. pTOS levels were not changed after the standardized mixed meal (Extended Data Fig. 3e). Therefore, across the six available human meal-test datasets, five showed that pTOS increases after a meal. The single exception involved participants with prediabetes or type 2 diabetes. We conclude that pTOS is present in the circulation in humans. In addition, a modest postprandial induction of pTOS in

https://doi.org/10.1038/s42255-026-01485-0

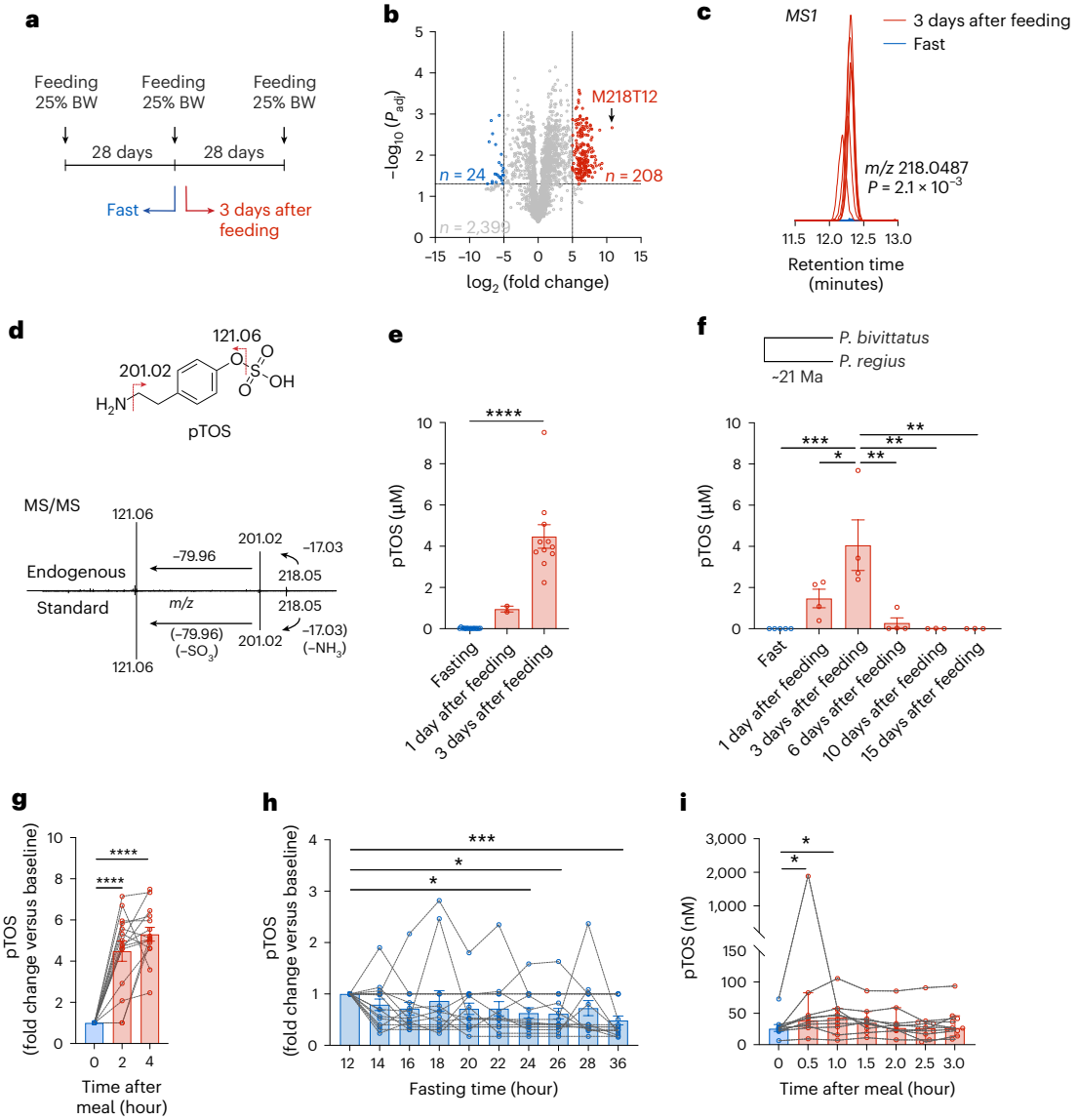

Fig. 1 | Postprandial pTOS increase in python and human plasma. a, Feeding scheme of Burmese pythons (*P. molurus bivittatus*) and the time points of blood plasma collection. **b**, Global changes in metabolites between 3 days after feeding and 28-day fasted Burmese python plasma using untargeted metabolomics ($n = 6$ per group). **c**, Extracted ion chromatograms of the $m/z = 218.0487$ from fasting and plasma 3 days after feeding. **d**, Chemical structure of pTOS (top) and MS/MS fragmentation of the endogenous $m/z = 218.0487$ and authentic pTOS standard (bottom). **e**,**f**, Absolute quantitation of pTOS in Burmese (**e**) and ball (*P. regius*) (**f**) pythons at the indicated time point. **g**, Relative changes of pTOS levels in human plasma with the recovery standardized liquid diet meal in the 'HuMet' study ($n = 15$ humans). **h**, Relative changes of pTOS levels in human plasma with fasting in the 'HuMet' study ($n = 15$ humans). **i**, Absolute quantitation of pTOS in human plasma after three mixed meal tests in the 'Voldstedlund' study ($n = 10$ humans). **e**, $n = 15$ for the fasting group, $n = 2$ for the 1 day after feeding group, $n = 11$ for the 3 days after feeding group. **f**, $n = 5$ for the fasting group, $n = 4$ for the 1 day, 3 days and 6 days after feeding groups, $n = 3$ for the 10 days and 15 days after feeding groups. **e**–**h**, Data are shown as the mean ± s.e.m. **b**,**c**, *P* values were calculated with two-tailed *t*-tests and adjusted with the Benjamini–Hochberg method. **e**,**f**, *P* values were calculated using a one-way analysis of variance (ANOVA) followed by Turkey's multiple comparison tests. **g**,**h**, *P* values were calculated with a repeated measures one-way ANOVA followed by Dunnett's multiple comparisons test. **i**, Data are shown as the median ± 95% confidence intervals. *P* values were calculated with a two-sided Friedman test followed by Dunn's multiple comparisons test. $*P < 0.05$, $**P < 0.01$, $***P < 0.001$, $****P < 0.0001$. Exact P values are as follows: **e**, fasting versus 3 days after feeding, $P = 1.5 \times 10^{-5}$; **f**, fasting versus 3 days after feeding, $P = 0.0006$, 1 day after feeding versus 3 days after feeding, $P = 0.0440$, 3 days after feeding versus 6 days after feeding, $P = 0.0021$, 3 days after feeding versus 10 days after feeding, $P = 0.0022$ and 3 days after feeding versus 15 days after feeding, $P = 0.0022$; **g**, 0 versus 2, $P = 2.5 \times 10^{-8}$, 0 versus 4, $P = 3.0 \times 10^{-10}$; **h**, 12 versus 24, $P = 0.0304$, 12 versus 26, $P = 0.0226$, 12 versus 36, $P = 0.0008$; **i**, 0 versus 0.5, $P = 0.0312$, 0 versus 1, $P = 0.0161$.

humans is generally observed across most studies but may be absent in participants with impaired glucose homeostasis.

To independently verify postprandial induction of pTOS in humans and to quantitatively determine absolute concentrations of pTOS in circulation, we used liquid chromatography (LC)–MS to measure pTOS levels from blood samples that had been previously collected during a meal test led by Voldstedlund et al.[24] In this study, ten healthy male participants were fasted for 6.5 h and then consumed three mixed-nutrient meals (one solid, two liquid). Plasma was collected in the fasted state and at several time points after initiation of the first meal. We quantified plasma pTOS levels to be ~25 nM in the fasted state and increased by an average twofold after the meal (Fig. 1i), with one individual exhibiting a more than 25-fold increase of pTOS and circulating concentrations of ~2 μM at 0.5 h after the meal.

Lastly, we examined circulating pTOS levels in mice. Surprisingly, we did not robustly detect pTOS in mouse plasma either in the basal state or after a meal (Extended Data Fig. 3f; limit of detection less than 1 nM). We also surveyed publicly available datasets of human, mouse or rat blood metabolomics. pTOS was reported in 20 of 537 human studies (4%) but in none of 237 mouse and none of 52 rat studies (Extended Data Fig. 3g). On the other hand, the amino acid tyrosine was detected with equal frequency in metabolomics datasets from all three species (39% human, 34% mouse, 33% rat) (Extended Data Fig. 3h). We conclude that pTOS is not present, or at very low less than 1-nM levels, in mouse blood.

Python biosynthesis of pTOS from dietary tyrosine

To understand the mechanisms underlying the dramatic postprandial induction of pTOS in pythons, we sought to understand the pathways of pTOS biosynthesis. The structural similarity between pTOS and the amino acid tyrosine suggests a sequential biosynthesis pathway involving decarboxylation of the dietary amino acid tyrosine to produce tyramine, followed by sulfation to generate pTOS (Fig. 2a). When we administered tyrosine to fasted ball pythons (1 g kg^{-1} orally), we observed a 5.1-fold increase in plasma pTOS levels after 24 h compared to vehicle controls (Fig. 2b). We conclude that dietary tyrosine can be metabolically converted to pTOS in pythons. This rise, although significant, was less pronounced than the postprandial response, probably because the extensive gastrointestinal remodelling that accompanies feeding (including increased blood flow to the gut and upregulation of amino acid transporters) probably does not occur during acute tyrosine gavage.

We next focused on each step of the tyrosine–pTOS pathway. The first tyrosine decarboxylation step can be catalysed by several enzymes, the most well-studied of which are bacterial tyrosine decarboxylases (TDCs) (EC 4.1.1.25)[25]. These enzymes exhibit high affinity and specificity for tyrosine and are highly expressed in several gut bacterial taxa, such as the *Lactobacillus* and *Enterococcus* species. Therefore, we isolated and cultured fecal bacteria from ball pythons in standard amino acid complete (SAAC) medium and examined the production of pTOS in vitro. Addition of tyrosine (50 mM) and the cofactor pyridoxal 5′-phosphate (5 mg l^{-1}) for 2 days significantly increased tyramine production in both cells and medium compared to cells that were not treated with tyrosine starting material (Fig. 2c). When we further isolated and cultured bacteria from ball python small and large intestines under fasted or fed conditions, we observed exclusive tyramine production from large intestine microbes, which was further enhanced in the fed versus fasted condition (Fig. 2d).

Next, we examined the second step of tyramine sulfation. Sulfotransferases (SULTs) are a class of enzymes that catalyse metabolite sulfation and exhibit liver-enriched expression[26]. We reasoned that python hepatic SULT activity may mediate conversion of tyramine to pTOS. Consistent with this premise, robust production of pTOS was observed after the addition of tyramine to liver tissue slices that had been freshly isolated from fasted pythons (Fig. 2e). When similar experiments were performed using liver tissue slices isolated from pythons 3 days after feeding, pTOS production was further increased (Fig. 2e). We performed tandem mass tag (TMT)-based quantitative proteomics analysis on the liver from fasted, 1 day after feeding and 3 days after feeding pythons (Fig. 2f,g and Supplementary Table 2). We observed significant increases in the abundance of python hepatic enzymes involved in metabolite sulfation reactions. For instance, two 3′-phosphoadenosine 5′-phosphosulphate (PAPS) synthases, which provide the sulphur donor in these reactions, were increased by 2–20-fold in the postprandial state (Fig. 2h). In addition, four SULTs were also increased by 2–6-fold (Fig. 2i). To determine if any of these python SULTs could catalyse tyramine sulfation, we expressed individual python SULT enzymes in HEK 293T cells and tested cell lysates for SULT activity. We confirmed expression of python SULT1A1, SULT1C4 and SULT6B1 by anti-FLAG immunoblotting, while python SULT1D1 failed to express under these conditions. Cell lysates expressing python SULT1C4, but not SULT1A1 or SULT6B1, exhibited robust tyramine sulfation activity (Fig. 2j). We conclude that a two-step biochemical pathway in pythons involving decarboxylation and hepatic sulfation converts dietary tyrosine to pTOS.

Lastly, we sought to critically test the requirement of gut bacteria in postprandial pTOS production in pythons. Therefore, we treated pythons with a cocktail of antibiotics (ABX) (200 mg kg^{-1} metronidazole, 200 mg kg^{-1} ampicillin, 100 mg kg^{-1} neomycin and 100 mg kg^{-1} erythromycin) and measured pTOS levels after a meal. ABX-mediated depletion of the gut microbiome was confirmed by reduced gut bacterial content (Extended Data Fig. 4a,b). Control pythons exhibited expected postprandial increase of pTOS (Fig. 2k). This rise in pTOS was largely abolished in ABX-treated pythons (Fig. 2k). We conclude that gut bacteria are required for postprandial pTOS induction in pythons.

pTOS suppresses feeding behaviours in mice

No biological function has been attributed to pTOS. Its dramatic induction in the python postprandial phase prompted us to investigate whether pTOS might influence whole-body energy metabolism. We performed gain-of-function experiments by administering pTOS (50 mg kg^{-1}, intraperitoneally) to male mice in metabolic chambers. Such a dose was chosen to achieve circulating pTOS levels that are comparable to postprandial python levels. Under these conditions, we observed an increase in plasma pTOS levels that peaked at 11.4 ± 1.2 μM at 1 h, and decreased to 2.9 ± 0.6 μM at 2 h and 0.5 ± 0.1 μM at 4 h (Extended Data Fig. 5a). Mice treated with pTOS exhibited a significant reduction in food intake (mean ± s.e.m.; vehicle: 4.39 ± 0.28 g, pTOS: 3.58 ± 0.16 g, $P = 0.024$) over the 24-h period (Fig. 3a,b). While the respiratory exchange ratio (RER) trended towards lower in pTOS-treated mice, this difference was not statistically significant (Fig. 3c,d). It may also be possible that other, more subtle aspects of glucose metabolism are concurrently altered in pTOS-treated mice, leading to an increased RER above what would be expected from reduced feeding. Energy expenditure (Fig. 3e,f and Extended Data Fig. 5b–d) and locomotor activity (Fig. 3g,h) were also not statistically different between vehicle-treated and pTOS-treated mice. Importantly, pTOS administration did not affect water intake (Fig. 3i), induce conditional flavour avoidance (Fig. 3j and Extended Data Fig. 5e) or affect sucrose preference (Fig. 3k). pTOS administration also did not alter blood glucose levels (Extended Data Fig. 5f).

We performed additional experiments to characterize the anorexigenic effect of pTOS in mice. In a 3-h feeding experiment, pTOS (50 mg kg^{-1}, intraperitoneally) reduced food intake in both lean (vehicle: 1.01 ± 0.04 g, pTOS: 0.73 ± 0.03 g, $P = 5 \times 10^{-4}$) and diet-induced obese (DIO) (vehicle: 0.64 ± 0.07 g, pTOS 0.30 ± 0.03 g, $P = 0.003$) male mice housed in home cages (Fig. 3l,m). Oral gavage administration of pTOS (50 mg kg^{-1}, orally) also increased plasma pTOS levels (Extended Data Fig. 5g) and reduced 3-h food intake in both lean (vehicle: 1.13 ± 0.08 g, pTOS 0.90 ± 0.04 g, $P = 0.030$) and DIO (vehicle: 0.80 ± 0.05 g, pTOS: 0.60 ± 0.05 g, $P = 0.015$) male mice (Fig. 3n,o). The higher exposure levels of pTOS after oral gavage versus intraperitoneal administration may be due to its partitioning to fat/mesenteric tissues, which could slow its systemic release. The effect of pTOS on food intake was dose-dependent (Fig. 3p and Extended Data Fig. 5h). Chronic administration of pTOS (50 mg kg^{-1}, intraperitoneally) to DIO mice durably reduced daily food intake (vehicle: 2.25 ± 0.09 g, pTOS: 2.00 ± 0.07 g, $P = 0.049$) (Fig. 3q) and produced a −9% vehicle-adjusted reduction in body weight (vehicle: 2.59 ± 0.68 g, pTOS: −0.87 ± 0.57 g, $P = 0.002$) (Fig. 3r). We conclude that pTOS non-aversively reduces food intake and obesity without affecting water intake, energy expenditure or movement.

Because pTOS is a sulfated tyramine analogue, and because tyramine has been previously shown to suppress feeding[27,28], we next sought to determine whether the anorexigenic activity of pTOS might be mediated by a tyraminergic activity of this metabolite. Using a cyclic AMP-based

https://doi.org/10.1038/s42255-026-01485-0

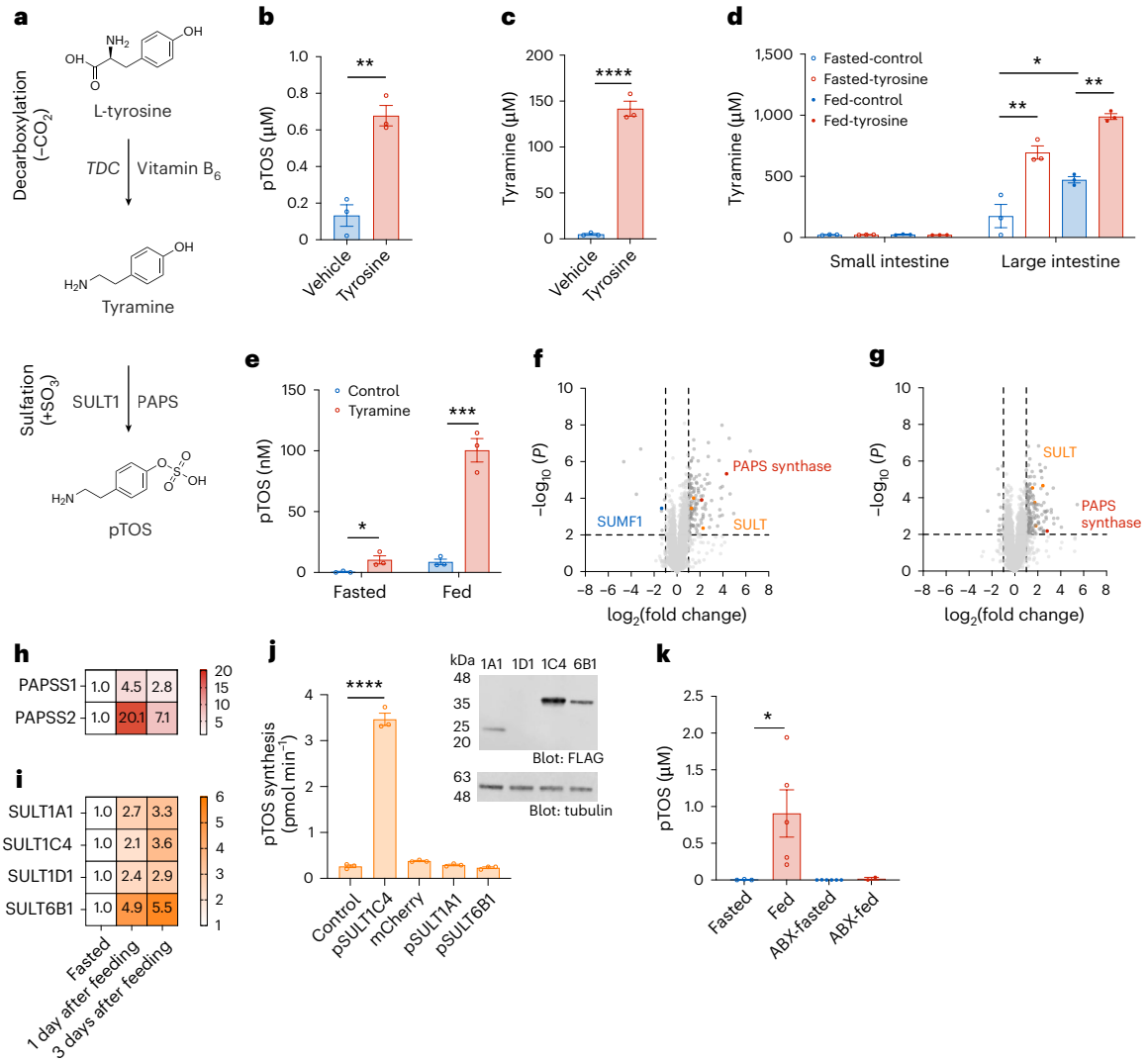

Fig. 2 | pTOS production from dietary tyrosine. a, Scheme of the biochemical reactions involved in pTOS synthesis. Dietary tyrosine is converted to pTOS through decarboxylation and subsequent sulfation. **b**, Plasma pTOS levels in fasted (28 days after feeding) ball pythons 1 day after tyrosine (1 g kg^{-1}) or vehicle oral gavage ($n = 3$ per group). **c**, Tyramine levels in the media of anaerobic bacterial cultures of ball python feces using the SAAC medium (control, containing 1 mM tyrosine and 0.1 mg l^{-1} vitamin B_6) or supplemented with 50 mM tyrosine and 5 mg l^{-1} vitamin B_6 (tyrosine) ($n = 3$ per group). **d**, Tyramine levels in the Gifu medium of anaerobic cultures of the microbiome collected from the small and large intestines of fasted (107 days after feeding) or fed (3 days after feeding) ball pythons ($n = 3$ per group). **e**, pTOS levels in the conditioned medium of python liver slices incubated with tyramine (1 mM) or vehicle for 16 h. Livers were freshly isolated from fasted (31 days after feeding) or fed (3 days after feeding) ball pythons ($n = 3$ per group). **f**,**g**, Proteomic changes in the livers of fasted versus 1 day after feeding (**f**) and fasted versus after 3 days after feeding (**g**) ball pythons at the indicated time point. **h**,**i**, Fold changes of PAPS synthases (**h**) and SULTs (**i**) in livers at the indicated time point. Fasted liver samples were normalized to 1. **f**–**i**, $n = 5$ for the fasting and 1 day after feeding groups, $n = 4$ for the 3 days after feeding group. **j**, Sulfation activity of HEK 293T cell lysates expressing FLAG-tagged python SULTs, using tyramine as the substrate. Immunoblot analysis shows the expression of the python SULTs (anti-FLAG, top) and loading control (anti-tubulin, bottom). **k**, Plasma pTOS levels in fasted (28 days after feeding) or fed (3 days after feeding) Burmese pythons after ABX treatment. Vehicle-treated pythons: $n = 3$ for fasted, $n = 5$ for fed; ABX-treated pythons: $n = 6$ for fasted, $n = 2$ for fed. SUMF1, sulfatase-modifying factor 1. Data are shown as the mean ± s.e.m. **b**,**c**, P values were calculated with two-tailed t-tests. **d**, P values were calculated with a one-way ANOVA followed by Holm-Šidák's multiple comparisons test. **e**, P values were calculated with multiple two-tailed t-tests. **f**,**g**, P values were calculated with two-tailed t-tests adjusted with the Benjamini–Hochberg method. **j**, P values were calculated with a one-way ANOVA followed by Dunnett's multiple comparisons test. **k**, P values were calculated with a one-way ANOVA followed by Bonferroni's multiple comparisons test. $^*P < 0.05$, $^{**}P < 0.01$, $^{***}P < 0.001$, $^{****}P < 0.0001$. Exact P values are as follows: **b**, $P = 0.002$; (**c**) $P = 7.5 \times 10^{-5}$; **d**, Large intestine, fasted-control versus fasted-tyrosine, $P = 0.001$, fasted-control versus fed-control, $P = 0.0192$, fed-control versus fed-tyrosine, $P = 0.001$; **e**, fasted, $P = 0.0424$, fed, $P = 0.0007$; **j**, control versus pSULT1C4, $P = 2.1 \times 10^{-11}$; **k**, fasted versus fed, $P = 0.0234$.

cellular assay, we were unable to detect pTOS-dependent activation of the trace amine-associated receptor TAAR1 (ref. 29) (Extended Data Fig. 5i). In addition, administration of pTOS (50 mg kg^{-1}, intraperitoneally) to mice did not increase blood pressure (Extended Data Fig. 5j), whereas tyramine itself (50 mg kg^{-1}, intraperitoneally) was, as expected, vasoactive in this assay (Extended Data Fig. 5k)[30]. We conclude that pTOS does not exhibit tyraminergic activity.

pTOS may also affect feeding by regulating the levels of other hormones previously implicated in food intake control. However, we did not detect any changes in plasma ghrelin (Extended Data Fig. 5l), leptin (Extended Data Fig. 5m), adiponectin (Extended Data Fig. 5n), insulin (Extended Data Fig. 5o), glucagon-like-peptide-1 (GLP-1) (Extended Data Fig. 5p) or GDF15 (Extended Data Fig. 5q) levels at either 1 h or 3 h after pTOS administration. pTOS did not affect

https://doi.org/10.1038/s42255-026-01485-0

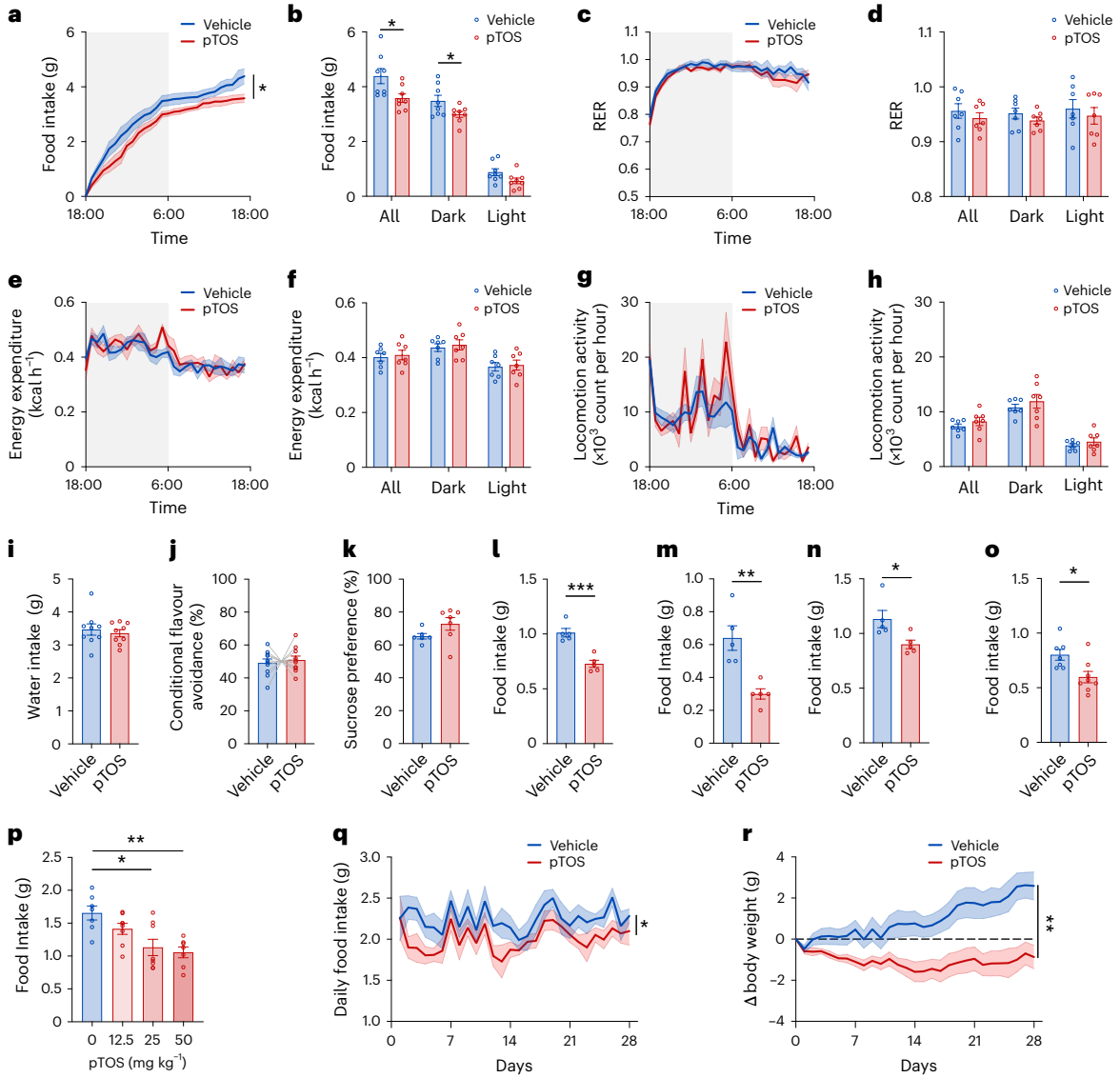

Fig. 3 | Effects of acute pTOS administration to mice. a–**h**, Metabolic parameters measured with 24-h fasted 16-week-old male mice treated with pTOS (50 mg kg^{-1}, intraperitoneally) or vehicle control. **a**,**b**, Cumulative food intake (**a**) and food intake during the light and dark cycles (**b**) ($n = 8$ per group). **c**,**d**, RER over time (**c**) and during the dark and light cycles (**d**) ($n = 7$ per group). **e**,**f**, Energy expenditure (adjusted for body mass) over time (**e**) and during the dark and light cycles (**f**) ($n = 7$ per group). **g**,**h**, Locomotor activity over time (**g**) and during the dark and light cycles (**h**) ($n = 7$ per group). **i**, Water intake (24 h) in 16-week-old male mice treated with pTOS (50 mg kg^{-1}, intraperitoneally) or vehicle control ($n = 9$ per group). **j**, Conditioned flavour avoidance ratio in paired solution for 8-week-old male mice treated with pTOS (50 mg kg^{-1}, intraperitoneally) or vehicle control ($n = 10$ per group). **k**, Sucrose preference ratio in 14-week-old male mice treated with pTOS (50 mg kg^{-1}, intraperitoneally) ($n = 7$) or vehicle control ($n = 6$). **l**,**m**, Three-hour food intake in lean (**l**, fed ad libitum, 12–14-week-old) and DIO (**m**, fed ad libitum, 14–15-week-old, 8–9 weeks on an HFD; body weights were: vehicle 37.0 ± 2.5 g, pTOS 37.4 ± 0.7 g) male mice treated with pTOS (50 mg kg^{-1}, intraperitoneally) or vehicle control ($n = 5$ per group). **n**,**o**, Three-hour food intake in lean (**n**, $n = 5$, 11–13-week-old) and DIO (**o**, $n = 7$ for vehicle, $n = 8$ for pTOS, 13–15-week-old, 7–9 weeks on HFD, body weights were: vehicle 34.1 ± 1.2 g, pTOS 34.1 ± 1.0 g) male mice (fed ad libitum) treated with pTOS (50 mg kg^{-1}, orally) or vehicle control. **p**, Three-hour food intake in lean (fed ad libitum, 14-week-old) male mice treated with pTOS or vehicle (intraperitoneally) at the doses indicated ($n = 7$ for 0 and 50 mg kg^{-1}, $n = 8$ for 12.5 and 25 mg kg^{-1}). **q**,**r**, Daily food intake (**q**) and body weight change (**r**) of DIO mice (16 weeks old, 8 weeks on HFD, body weights were: vehicle 37.8 ± 3.3 g, pTOS 40.0 ± 3.0 g) with daily pTOS injections (50 mg kg^{-1}, intraperitoneally) over a 28-day period. Data are shown as the mean ± s.e.m. **a**,**c**,**e**,**g**,**q**,**r**, P values were calculated using a two-way ANOVA. **b**,**d**,**f**,**h**,**i**,**j**,**k**,**l**,**m**,**n**,**o**, P values were calculated using two-sided t-tests. **p**, P values were calculated using a one-way ANOVA followed by Šídák's multiple comparisons test. $^*P < 0.05$, $^{**}P < 0.01$, $^{***}P < 0.001$. Exact P values are as follows: **a**, $P = 0.041$; **b**, all, $P = 0.0236$, dark, $P = 0.0499$, light, $P = 0.0741$; **l**, $P = 0.0005$; **m**, $P = 0.0031$; **n**, $P = 0.0303$; **o**, $P = 0.0150$; **p**, 0 versus 25, $P = 0.0034$, 0 versus 50, $P = 0.0013$; **q**, $P = 0.0494$; **r**, $P = 0.0062$.

systemic nutrient absorption after oral glucose, lipid or protein administration (Extended Data Fig. 6a–f). pTOS also did not affect gastric emptying, whereas exenatide, a GLP-1R agonist and positive control, showed the expected delayed emptying effect (Extended Data Fig. 6g). We conclude that the anorexigenic activity of pTOS is not dependent on changes in other known feeding-regulating hormones or on changes to gastric emptying or nutrient handling.

VMH neurons mediate the anorexigenic activity of pTOS

Feeding behaviours are controlled centrally. To determine if pTOS might act directly on the brain, we measured metabolite levels in cerebrospinal fluid (CSF) and whole-brain lysates after administration of either pTOS or tyramine control (50 mg kg^{-1}, intraperitoneally) to mice. Unlike tyramine administration, which led to low peak plasma levels (Extended Data Fig. 6h) and low accumulation

https://doi.org/10.1038/s42255-026-01485-0

of tyramine in either CSF (Extended Data Fig. 6i) or brain lysates (Extended Data Fig. 6j), pTOS was robustly detected after pTOS administration both in the CSF (at 12.6 µM; Extended Data Fig. 6k) and in total brain lysates (at 1.2 µM; Extended Data Fig. 6l) 30 min after administration. We conclude that pTOS exhibits enhanced plasma stability and penetrates the central nervous system to levels that may affect feeding pathways.

To understand the neural populations that might be modulated by pTOS, we performed activity mapping using the targeted recombination in active populations (TRAP) approach. We generated *TRAP2/Rosa26-LSL-tdTomato* mice[31] (Methods), which enable cFos-dependent recombination and genetic labelling of pTOS-activated neural populations with a tdTomato fluorescent reporter. *TRAP2/Rosa26-LSL-tdTomato* mice were treated with vehicle or pTOS (50 mg kg^{-1}, intraperitoneally) followed by 4-hydroxytamoxifen (4-OHT) (50 mg kg^{-1}, intraperitoneally) to induce recombination. Two weeks later, we collected the brains and examined multiple hypothalamic and brainstem regions for tdTomato$^+$ signals (Extended Data Fig. 7). pTOS treatment increased the number of tdTomato$^+$ cells in both the VMH (Fig. 4a,b) and the paraventricular hypothalamus (PVH) (Extended Data Fig. 7b). On the other hand, the number of tdTomato$^+$ cells was not statistically different between groups in the other brain regions examined (Extended Data Fig. 7c–m).

Next, we sought to determine whether the activation of VMH or PVH neurons was functionally relevant for the anorexigenic activity of pTOS. Therefore, we used viral approaches to enable chemical silencing of pTOS-activated neurons in these brain regions with the synthetic ligand clozapine-*N*-oxide (CNO) (Fig. 4c). To first target pTOS-activated neurons in the VMH, we stereotaxically injected a Cre-dependent adeno-associated virus (AAV) carrying the inhibitory designer receptors exclusively activated by designer drugs (DREADD) hM4Di-mCherry[32,33] bilaterally into the VMH of *TRAP2* mice. Two weeks later, DREADD expression was induced in pTOS-activated VMH neurons (hM4Di^{VMH}) using sequential administration of pTOS (50 mg kg^{-1}, intraperitoneally) and 4-OHT (50 mg kg^{-1}, intraperitoneally) (Fig. 4d) As controls, similar procedures were performed in wild-type (WT) littermates. In an acute feeding assay, pTOS, as expected, suppressed food intake in three groups: control mice pretreated with saline (mean ± s.e.m., vehicle: 1.55 ± 0.11 g, pTOS: 1.14 ± 0.05 g, $P = 0.007$), control mice pretreated with CNO (vehicle: 1.56 ± 0.12 g, pTOS: 1.22 ± 0.12 g, $P = 0.036$) and hM4Di^{VMH} mice pretreated with saline (vehicle: 1.60 ± 0.14 g, pTOS: 1.20 ± 0.11 g, $P = 0.048$; Fig. 4e). On the other hand, the anorexigenic effect of pTOS administration was blunted in CNO-pretreated hM4Di^{VMH} mice (vehicle: 1.54 ± 0.12 g, pTOS: 1.36 ± 0.08 g, $P = 0.093$; Fig. 4f). We conclude that pTOS-activated VMH neurons are required for the anorexigenic effects of pTOS.

To determine whether pTOS activates hM4Di^{VMH} neurons via a direct or indirect mechanism, we used post hoc slice electrophysiology to examine the activity of pTOS on these neurons in vitro. As a positive control, we first validated that in vitro treatment of hM4Di^{VMH} neurons with CNO reduced activity as expected (Fig. 4g). Next, we observed that pTOS treatment (1 µM) of hM4Di^{VMH} neurons in vitro increased neuronal firing (vehicle: 1.88 ± 0.55 Hz; pTOS: 2.46 ± 0.61 Hz), an effect that was reduced after pTOS removal during the washout period (1.67 ± 0.60 Hz; Fig. 4h). Furthermore, pTOS-dependent activation of hM4Di^{VMH} neurons persisted in the presence of a cocktail of synaptic blockers (Fig. 4i). We conclude that pTOS directly activates hM4Di^{VMH} neurons in vitro.

We next turned to examine the role of pTOS-activated PVH neurons. We performed similar experiments to those described above, but via stereotaxic injection of hM4Di-mCherry virus bilaterally into the PVH of *TRAP2* or WT control mice, rather than the VMH (Extended Data Fig. 8a). In this experiment, pTOS administration equally suppressed food intake in all four groups of mice (Extended Data Fig. 8b,c). We confirmed the efficiency of hM4Di-mediated inhibition of hM4Di^{PVH} neurons using post hoc slice electrophysiology (Extended Data Fig. 8d–f). Thus, the targeted subset of PVH neurons, although activated by pTOS, are not required to mediate the effect of pTOS on feeding behaviours.

Effect of pTOS on VMH neurons in pythons

Lastly, we sought to examine the effects of pTOS administration in pythons. Pythons eat in a single bout; consequently, the rate of feeding is difficult to directly measure in these animals. As a surrogate molecular marker of pTOS activity, we examined brain cFos levels using immunofluorescence 90 min after administration of pTOS (50 mg kg^{-1}, orally) or vehicle to ball pythons. The brain of the ball python is elongated along the sagittal plane, adapting to its narrow skull and predatory lifestyle (Fig. 4j). The python VMH was easily identifiable as a distinct oval cluster of neurons located in the hypothalamus, near the third ventricle (Fig. 4k)[34]. pTOS administration increased cFos staining in the VMH of ball pythons (Fig. 4l,m). We conclude that pTOS activation of VMH neurons is a conserved activity across species.

In addition to the VMH, we also examined cFos staining after pTOS treatment in other brain regions. These other regions were identified using standard anatomical markers[34]. We observed that many other brain regions showed similar cFos immunoreactivity between vehicle and pTOS groups (Extended Data Fig. 9). We also observed

Fig. 4 | Role of VMH neurons in the anorexigenic effects of pTOS. **a**, Anatomical location (left) and representative immunofluorescence section (right) of pTOS-activated neurons in the VMH in 10-week-old male *TRAP2/Rosa26-LSL-tdTomato* mice after treatment with vehicle or pTOS (50 mg kg^{-1}, intraperitoneally, $n = 3$ per group). **b**, Quantification of pTOS-activated neurons in **a**. **c**, Schematic illustration of using hM4Di-DREADD to suppress pTOS-activated VMH neurons in TRAP2 mice. Cre-dependent AAVs carrying hM4Di-mCherry DREADD were targeted to the VMH of TRAP2 mice for chemogenetic silencing. **d**, Representative image of hM4Di-mCherry expression in the VMH of male hM4Di^{PVH} mice; the experiment was repeated seven times with similar results. **e**,**f**, Food intake (4-h) in 13–14-week-old control or hM4Di^{VMH} mice pretreated with saline (**e**) or CNO (**f**), followed with pTOS (50 mg kg^{-1}, intraperitoneally) or vehicle administration ($n = 7$ per group). **g**, Representative image for electrophysiological recordings (top), representative action potential traces (middle) and quantitation of firing rate and resting membrane potential (bottom) of hM4Di^{VMH} neurons in response to CNO (10 µM, $n = 6$ neurons). **h**,**i**, Representative action potential traces (top) and quantitation of firing rate and resting membrane potential (bottom) of hM4Di^{VMH} neurons after treatment with pTOS (1 µM) in the absence (**h**) or presence (**i**) of synaptic blockers (30 µM cyanquixaline (CNQX), 30 µM 5-phosphono-D-norvaline (D-AP5) and 50 µM bicuculline) ($n = 10$ neurons per group). **j**, Schematic drawing of the sagittal view of a ball python brain (adapted from ref. 52). **k**, Coronal view of the brain section showing the VMH region. **l**, Representative cFos staining in the VMH of fasted ball pythons treated with pTOS (50 mg kg^{-1}, orally) or vehicle control. **m**, Quantitation of cFos$^+$ neurons in the VMH of ball pythons treated with pTOS (50 mg kg^{-1}, orally) or vehicle control ($n = 4$ per group). Data are shown as the mean ± s.e.m. **b**,**m**, P values were calculated using two-sided t-tests. **e**,**f**, P values were calculated using one-sided paired t-tests. **g**, P values were calculated using two-sided paired Wilcoxon signed-rank tests. **h**,**i**, P values were calculated using a one-way ANOVA followed by Turkey's multiple comparisons tests. *$P < 0.05$, **$P < 0.01$, ***$P < 0.001$. Exact P values are as follows: **b**, $P = 0.0464$; **e**, control, $P = 0.0070$, hM4Di^{VMH}, $P = 0.0483$; **f**, control, $P = 0.0358$, hM4Di^{VMH}, $P = 0.0929$; **g**, firing rate, $P = 0.0312$, membrane potential, $P = 0.0312$; **h**, firing rate, baseline versus pTOS, $P = 0.0369$, pTOS versus washout, $P = 0.0107$, membrane potential, baseline versus pTOS, $P = 0.0052$, pTOS versus washout, $P = 0.0220$; **i**, firing rate, baseline versus pTOS, $P = 0.0124$, pTOS versus washout, $P = 0.0264$, membrane potential, baseline versus pTOS, $P = 0.0002$, pTOS versus washout, $P = 0.0132$; **m**, $P = 0.0020$. Ch, cerebral hemisphere; cr, cerebellum; DAPI, 4′,6-diamidino-2-phenylindole; hypo, hypothalamus; mo, medulla oblongata; ob, olfactory bulb; ot, optic tectum; p, pituitary; II, second cranial nerve. **j**, Scale bar, 1 mm. **k**, Scale bar, 500 µm. **l**, Scale bar, 100 µm.

https://doi.org/10.1038/s42255-026-01485-0

that pTOS significantly inhibited neurons in the dorsal cortex, piriform cortex and spinal trigeminal nucleus (Extended Data Fig. 9b,c,l). Therefore, pTOS-dependent activation of python VMH neurons is specific to neurons in that region rather than reflecting a global increase in cFos activity after administration of this metabolite.

Discussion

Pythons exhibit extreme feeding and fasting patterns and provide a unique model system for uncovering molecular regulators of the postprandial response. Using pythons as a discovery tool, we provide multiple lines of evidence that pTOS is a postprandial

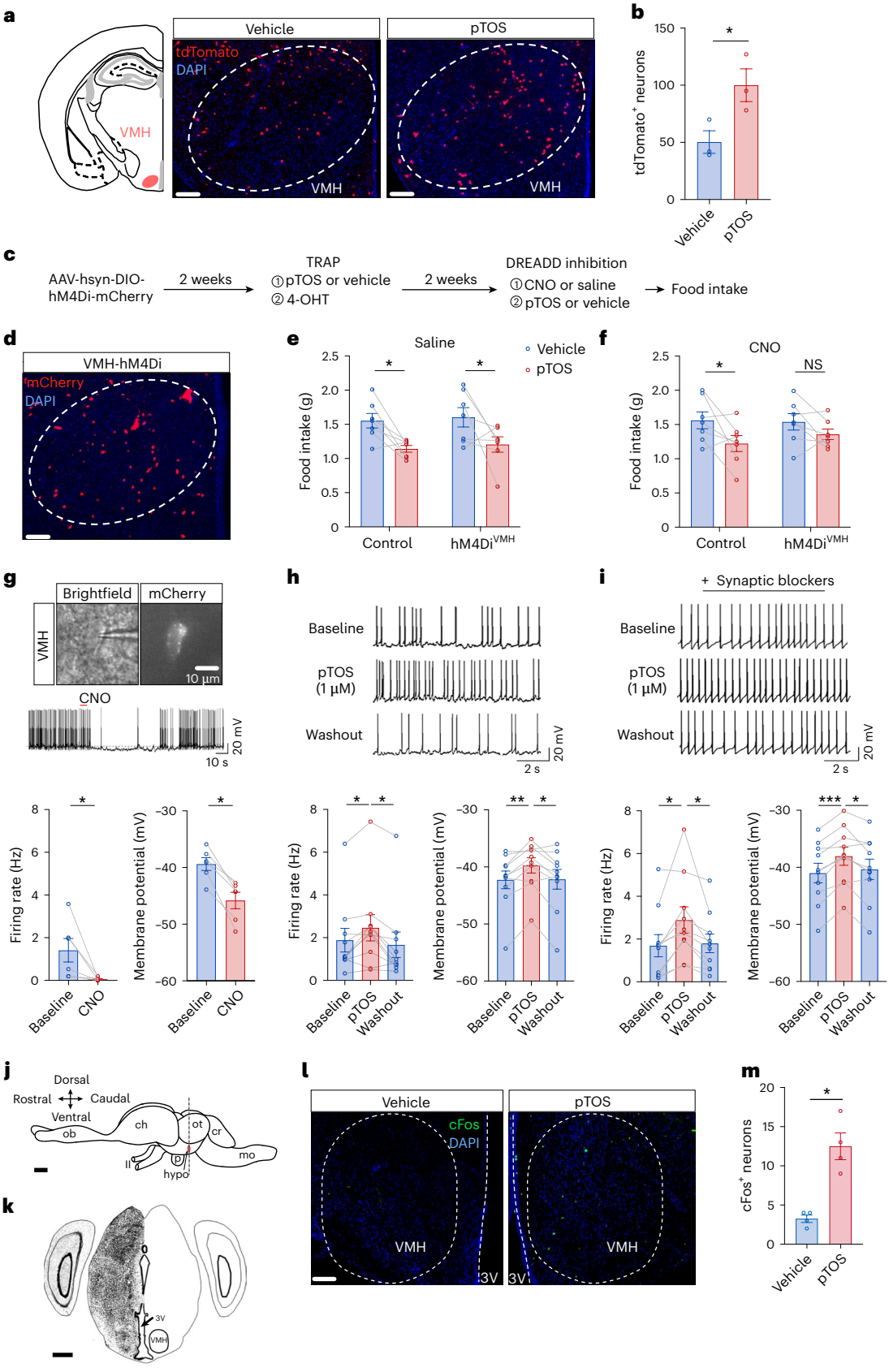

anorexigenic metabolite that links nutrient intake to feeding control: (1) circulating pTOS levels are induced by more than 1,000-fold after feeding in pythons; (2) python pTOS can be produced from microbiome-dependent metabolism of dietary tyrosine; (3) administration of pTOS to pythons activates a neural population in the VMH, a key region that controls feeding and energy homeostasis; (4) pTOS-dependent activation of VMH neurons in mice drives suppression of food intake, demonstrating conserved activity across species; and (5) pTOS is detectable in the circulation in humans and its levels are also increased after a meal. The discovery of the postprandial induction and central activity of pTOS underscores the power of extreme model organisms to uncover molecules that might otherwise be missed in more classical organisms, such as mammals, which exhibit more limited fluctuations of energy states and postprandial physiology.

Many other gut-derived peptide and protein hormones have been previously studied in the context of mammalian postprandial metabolism, including cholecystokinin, GLP-1, gastric inhibitory peptide, peptide YY and gastrin, and regulate diverse aspects of digestion, nutrient absorption, glucose regulation and feeding[34–36]. A growing body of recent work also suggests that gut-derived metabolites, such as bile acids and short-chain fatty acids, can have similarly important roles[35–37]. Our data nominate pTOS as a gut-derived metabolite with a critical role in the python postprandial response. In the future, it will be important to understand the time course of pTOS induction relative to the other known postprandial peptide hormones in pythons. It will also be important in the future to determine if pTOS might also interact with any of these other peptide hormone pathways, including GLP-1. Lastly, we show that pTOS activates a neural population in the VMH, a region that is integral to many neuroendocrine functions, including feeding and energy balance[38]. Projecting forward, the precise molecular identity of pTOS-activated VMH neurons, and the identity of specific downstream receptors within this cellular population that can be directly liganded by pTOS, still need to be identified. In addition, it is also possible that pTOS has additional bioactivity beyond feeding regulation alone.

Because pTOS is derived from dietary tyrosine, this metabolite can be considered a circulating sensor of tyrosine ingestion. It is possible that other dietary components, metabolic stimuli or endogenous secretions can also increase circulating pTOS levels. Currently the mechanisms responsible for the differing basal circulating levels of pTOS between Burmese and ball pythons, and humans, is unknown, but could reflect differences in production, tissue distribution, catabolism or clearance.

Chemically, pTOS is structurally related to tyramine, a monoamine metabolite and trace amine. Despite this structural similarity, sulfation functions as a chemical switch that fundamentally alters the pharmacological and physiological properties of tyramine to both inactivate tyraminergic activity and to confer neo-activities to pTOS, such as enhanced plasma stability and improved brain penetration. This chemical switch mechanism for tyramine and pTOS parallels that of acetylation and methylation for serotonin and melatonin and hydroxylation for dopamine and norepinephrine. All these chemical modifications and metabolite pairs underscore how small chemical changes can lead to profound effects on downstream function. The possibility that sulfation modifications may function as a general molecular switch for other metabolites is an interesting possibility that remains largely unexplored.

While pythons consistently exhibit the most dramatic induction of pTOS after a meal, we also observed postprandial induction of pTOS in humans. On average, pTOS levels were increased by ~2–5-fold after meals in most human cohorts examined. Nevertheless, we also found individuals with outlier pTOS responses: in the Mohold cohort study, one individual increased pTOS levels by more than 30-fold; in our own analysis of the Voldstedlund cohort study, another individual increased pTOS levels by more than 25-fold and reached python-level concentrations (~2 μM at 0.5 h after the meal). Therefore, postprandial regulation of pTOS is conserved in pythons and humans. In the future, it would be interesting to determine whether postprandial pTOS levels can be further augmented with larger, protein-enriched meals that more closely resemble the meals provided to pythons. It is also possible that the observed difference in induction levels reflects other physiological changes after feeding, given that humans do not undergo extensive gastrointestinal remodelling. In addition, the absence of pTOS in mice was surprising, considering its conservation in other species. We speculate that mice might instead produce a chemically related pTOS-like metabolite, which is analogous to how mice lack cortisol but use corticosterone as the functional equivalent[39].

Lastly, this work builds on the long tradition of harnessing reptiles for natural products and drug discovery. Snake venoms, for example, have yielded a large number of bioactive molecules with clinical significance, including peptide modulators of blood pressure (for example, angiotensin-converting enzyme inhibitors and angiotensin receptor antagonists) and potent antithrombotic proteins (for example, flavoridin and echistatin)[40–42]. Similarly, the Gila monster peptide exendin-4 paved the way for the development of exenatide, a first-generation GLP-1 receptor agonist[43]. Although these previous discoveries primarily focused on snake venom, our data show that snake blood can also be a rich source of new molecular entities. Dynamic physiological regulation, such as after a meal, can further help to identify high-priority candidates for downstream functional testing.

Methods

Python husbandry

The animal protocols and procedures involving pythons were approved by the Institutional Care and Use Committee of the University of Colorado Boulder. Captive-bred Burmese pythons (*P. molurus bivittatus*) and Ball pythons (*P. regius*) were purchased from Bob Clark Reptiles, Oklahoma City. Pythons were single-housed in the University of Colorado Boulder vivarium in 12-h light–dark cycles at 30 °C with 50% relative humidity. Pythons were then subjected to fasting and feeding schedules as in Fig. 1a, consisting of a 28-day fasting period followed by feeding with a meal equal to 25% of their body weight. Burmese pythons were approximately 2 years old and weighed 1.5–2.5 kg at the start of the study. Ball pythons were approximately 1 year old at the start of the experiments and weighed 400–500 g.

pTOS synthesis and purity

pTOS was synthesized according to the scheme in Supplementary Fig. 1. To a solution of compound 1 (40 g, 291.6 mmol, 1.0 eq) in tetrahydrofuran (THF) (2.0 l) at 0 °C, FmocCl was added (75.43 g, 291.6 mmol, 1.0 eq) in THF (1.0 ml). The mixture was stirred for 16 h. Once compound 1 was consumed completely, the mixture was adjusted to pH 1 with 1 N HCl. The mixture was extracted with ethyl acetate (800 ml ×3). The organic phase was washed with brine and dried over sodium sulfate, filtered and concentrated. The residue was triturated with dichloromethane, filtered and dried to afford compound 2 (49 g, 47%) as white solid. To a solution of compound 2 (10.0 g, 27.8 mmol, 1.0 eq) in dioxane (10 ml) in dimethylformamide (100 ml), SO_3-dimethylformamide (12.8 g, 83.4 mmol, 3.0 eq) and pyridine (20 ml) were added. The mixture was stirred for 16 h. Once compound 2 was consumed completely, the residue was adjusted to pH 8 with 5% aqueous $NaHCO_3$ solution. The mixture was concentrated and diluted with water (100 ml). The precipitate was filtered to afford white solid. The solid was purified using C18 (50% acetonitrile in water) and freeze-dried to obtain compound 3 (10.0 g, 78%) as white solid. To a solution of compound 3 (17.0 g, 36.9 mmol, 1.0 eq) in dioxane and water (1:1, 35 mL), $Pd(OH)_2/C$ (1.7 g) was added under N_2 atmosphere. The mixture was stirred under hydrogen atmosphere for 48 h (15 psi). Once compound 3 was consumed completely, the mixture was filtered through a pad of Celite and the filtration was concentrated. The residue was triturated with ethyl acetate, filtered and dried to afford pTOS

(7.7 g, 87%) as white solid with more than 95% purity using ^{1}H NMR (400 MHz) (Supplementary Fig. 2) and more than 96% purity using high-performance LC (Supplementary Fig. 3).

^{1}H NMR (400 MHz, D_2O) δ 7.35 (d, J = 8.1 Hz, 2H), 7.29 (d, J = 8.3 Hz, 2H), 3.00 (t, J = 6.9 Hz, 2H), 2.85 (t, J = 7.0 Hz, 2H).

Mouse husbandry

All mouse experiments were performed according to procedures approved by the Institutional Care and Use Committee of Stanford University and Baylor College of Medicine. Mice were maintained in 12-h light–dark cycles at 22 °C with 50% relative humidity. Mice were fed with a standard rodent chow diet (18% protein and 6% fat; Envigo Teklad 2018) or an HFD (60% kcal fat; cat. no. D12492, Research Diets), as specified.

Acute mouse feeding studies

Male mice aged 12–14 weeks (C57BL/6J, strain no. 000664) and 14–15 weeks (C57BL/6J DIO, strain no. 380050) were obtained from The Jackson Laboratory. DIO mice were placed on an HFD for 8–9 weeks since 6 weeks old. Standard rodent chow (18% protein, 6% fat; Envigo Teklad 2018) or an HFD (60% kcal from fat) were provided to lean or DIO mice, as specified. Mice were single-housed 3 h before the onset of the dark cycle with ad libitum access to food and water. At the onset of the dark cycle, mice received a pTOS intraperitoneal injection (50 mg kg^{-1} or as indicated in the figures) or oral gavage. Food weight was recorded at baseline (0 h) and after 3 h. The body weights of DIO mice were: intraperitoneal vehicle 37.0 ± 2.5 g, pTOS 37.4 ± 0.7 g; oral: vehicle 34.1 ± 1.2 g, pTOS 34.1 ± 1.0 g.

Chronic pTOS treatment in DIO mice

For the chronic treatment, WT C57BL/6J 8-week-old male mice were fed with an HFD (60% kcal from fat) for 8 weeks. The initial body weights of mice were: vehicle 37.8 ± 3.3 g, pTOS 40.0 ± 3.0 g. Mice were then single-housed and administered pTOS (50 mg kg^{-1}, intraperitoneally) or vehicle daily 3 h before the onset of the dark cycle for 28 executive days. The mixture of 18:1:1 (by volume) of saline was Kolliphor EL (cat. no. C5135, Sigma-Aldrich). Dimethyl sulfoxide (DMSO) (Kolliphor) was used as vehicle. Daily food and body weight were recorded.

Python feeding studies

Pythons were randomly assigned to different endpoint groups. They were then fasted for 28 days, after which they received a rat meal equivalent to 20–25% of their body weight. At each pre-assigned endpoint, pythons were euthanized via rapid decapitation under deep isoflurane-induced anaesthesia. Sufficient anaesthetic depth was confirmed by lack of response to physical stimuli. Blood was collected in BD Vacutainer Lithium Heparin tubes (Thermo Fisher Scientific), immediately mixed by inversion, placed on ice for 10 min and then plasma was separated by centrifugation at 3,000g for 15 min to pellet red blood cells. The supernatant was collected, flash-frozen in liquid nitrogen and stored at −80 °C until further analysis. Dissected tissues were rinsed in ice-cold PBS and then flash-frozen in liquid nitrogen and stored at −80 °C until further analysis.

Python oral gavage studies

Ball pythons were randomly assigned to experimental or control groups and then fasted for 28 days. Tyrosine, water or pTOS were then delivered by oral gavage using a 5 Fr. 16-inch rubber Sovereign Sterile Feeding Tube (MWI). Tyrosine was administered at 1 g kg^{-1} dissolved in water. pTOS was administrated at 50 mg kg^{-1} in an 18:1:1 mixture of water. Pythons that received pTOS or vehicle control were euthanized and dissected 90 min after gavage. Pythons that received tyrosine were euthanized and dissected 24 h after gavage. Plasma and tissues were collected as described above.

Human meal-test study (Voldstedlund study)

Arterial plasma samples were obtained from a meal-test study that was approved by the Research Ethics Committee of Copenhagen and published previously[24]. Briefly, ten young male individuals (age: 26.7 ± 1.3 years; BMI: 22.6 ± 0.6 kg m^{-2}) first performed a 60-min one-legged dynamic knee extensor exercise 90 min after a small breakfast (18 kJ per kg) in the morning. Four hours later (time '0 min'), individuals received a mixed solid meal (30 kJ per kg body weight), followed by two mixed liquid meals (20 kJ per kg body weight; Nutridrink, Nutrica) 30 min and 60 min after the solid meal. The mixed meals were composed of (energy intake) 50% carbohydrates, 35% fat and 15% protein.

Tyramine production from fecal samples

Fecal samples from ball pythons (21 mg) were dispensed in 500 µl SAAC medium, described previously[44]. The mixture was centrifuged at 100g for 5 min to pellet undigested materials. Then, 100 µl of the supernatant was mixed with 300 µl SAAC medium and incubated in an anaerobic chamber (Coy Laboratories) at 37 °C for 2 days, in an atmosphere of 5% hydrogen, 10% carbon dioxide and 85% nitrogen. Control SAAC medium contained 1 mM tyrosine and 0.1 mg l^{-1} vitamin B_6. Testing medium contained 50 mM tyrosine and 5 mg l^{-1} vitamin B_6. Cells were pelleted by centrifugation at 3,381g to separate bacteria from the conditioned medium. Then, 150 µl of 2:1:1 acetonitrile:methanol:water mixture was added to extract metabolites from the bacteria and 50 µl of medium were mixed with 150 µl 2:1 acetonitrile:methanol to extract the metabolites from medium.

Tyramine production from the python microbiome

Intestinal content was collected from the small and large intestines of a fed (3 days after feeding) and a fasted (107 days after feeding) python and stored at −80 °C. The intestinal content was then washed in reduced PBS supplemented with 0.05% cysteine and centrifuged at 100g for 5 min to pellet undigested materials. The supernatant was then centrifuged at 5,000g for 5 min to pellet bacteria. Bacteria were resuspended in 10 ml of reduced Gifu medium. A final concentration of 10 g l^{-1} tyrosine and 500 mg l^{-1} vitamin B_6 was used in the experimental group. Bacteria were cultured for 48 h at 30 °C in an anaerobic chamber. At the end of the incubation period, cells were pelleted by centrifugation at 5,000g for 5 min. The medium was collected for further LC–MS analysis.

Python ABX treatment

A cocktail of ABX containing 200 mg kg^{-1} metronidazole, 200 mg kg^{-1} ampicillin, 100 mg kg^{-1} neomycin and 100 mg kg^{-1} erythromycin was delivered to juvenile Burmese pythons (weighing 125–200 g at the time of the study) via oral gavage over a 7-day period. The ABX cocktail was administrated to pythons via oral gavage on days 1, 2, 3, 5 and 7. Control pythons received oral gavage of vehicle (water) at an equivalent volume. Concurrently, ABX-treated pythons also received metronidazole, ampicillin, neomycin and erythromycin (each at 0.1 g l^{-1}) in the drinking water. Seven days after the first dose of ABX, pythons were either euthanized or fed a mouse meal equal to 25% of their body weight. ABX-treated pythons received a germ-free mouse meal, whereas vehicle-treated pythons received a specific pathogen-free mouse meal. ABX-treated pythons continued to receive the antimicrobial cocktail via drinking water after their meal. Pythons were euthanized with or without ABX treatment at 3 and 28 days after feeding. Plasma was collected as described above.

Large intestinal content DNA quantification and gel visualization

The large intestinal contents of fasted and 3 days after feeding pythons were emptied; from them, DNA was isolated using the ZymoBIOMICS DNA Miniprep Kit. DNA from 5 mg of intestinal contents was mixed with 3 µl of Novex Hi-Density TBE Sample Buffer and electrophoresed using

a 10% (w/v) Novex TBE Gel for 1.5 h at 145 V. The gel was stained using 0.8 μg ml^{-1} ethidium bromide in water for 5 min; the gel was imaged using the UV setting on a Cytiva IQ 800 gel imager. Lanes within the gel were quantified using Fiji (Image J) and normalized to the average intensity of fasted, vehicle-treated pythons.

TMT-based proteomics of livers from ball pythons

Livers from fasted (n = 5), 1 day after feeding (n = 5) and 3 days after feeding (n = 4) ball pythons were collected as outlined above. Liver samples were homogenized with metal beads in lysis buffer (200 mM EPPS, pH 8.5, 8 M urea, 0.1% SDS, 1× protease inhibitors and 1× phosphatase inhibitors). The supernatant was collected after centrifugation at 21,130*g* for 10 min. Then, 25 μg of protein from each sample was reduced with tris(2-carboxyethyl)phosphine, alkylated with iodoacetamide and then further reduced with dithiothreitol. Proteins were precipitated onto SP3 beads and digested with Lys-C (1:25) overnight at room temperature, followed by trypsin (1:25) for 6 h at 37 °C. Peptides were labelled with TMT 18plex reagents. The, 2 μl of each sample was pooled and used to shoot a ratio check to confirm complete TMT labelling and to allow for normalization of each sample. All 14 TMTPro-labelled samples were pooled according to the ratios determined from the ratio check. Peptides were desalted using a Sep-pak and fractionated into 24 fractions using basic reverse-phase high-performance LC. Twelve fractions were solubilized, desalted by stage tip and analysed on an Orbitrap Eclipse mass spectrometer with a field asymmetric waveform ion mobility spectrometry device enabled. MS/MS spectra were searched using the COMET algorithm against a Python UniProt composite database containing its reversed complement and known contaminants. Peptide spectral matches were filtered to a 1% false discovery rate using the target-decoy strategy combined with linear discriminant analysis. The proteins were filtered to a less than 1% false discovery rate and quantified only from peptides with a summed signal-to-noise threshold greater than 140. A total of 6,389 proteins were quantified and used in the further analysis.

pTOS production with python liver slices

Fed (3 days after feeding) and fasted (31 days after feeding) ball pythons were euthanized via rapid decapitation while under anaesthesia and the liver was immediately collected and washed in sterile PBS. Freshly isolated liver was transferred to a sterile fume hood and 0.5 g of total liver mass was diced into fine segments (~2 × 2 mm) and then placed into one well of a 6-well plate containing 2 ml William's E medium supplemented with 1% non-essential amino acids, 1% GlutaMAX, 2% fasted python plasma, 100 nM dexamethasone, 100 nM insulin and 0.375% fatty-acid-free bovine serum albumin. Tyramine (1 mM final concentration) or vehicle control was added to the medium and incubated at 30 °C, 5% CO_2 for 16 h. The medium was collected and clarified by centrifugation at 21,130*g* for 10 min. The supernatant was flash-frozen in liquid nitrogen and stored at −80 °C until further analysis.

Python SULT expression in HEK 293T cells and enzymatic assay

Aryl SULTs with higher abundance in postprandial python livers were codon-optimized for expression in HEK 293T cells and synthesized by Integrated DNA Technologies. The sequences were then cloned into a pCMV5-mCherry vector with a 3× FLAG tag on the C terminal. For simplicity, we named the python SULTs with the following annotations based on the sequence similarities: SULT1A1 (A0A9F5IVD0), SULT1C4 (A0A9F2QWK4), SULT1D1 (A0A9F2REM3) and SULT6B1 (A0A9F2R4U1). HEK 293T cells were transiently transfected with Polyfect; 24 h later, cells were washed with ice-cold PBS and scraped into an Eppendorf tube. Cells were pelleted using centrifugation at 845*g* for 5 min at 4 °C and lysed in 50 mM potassium phosphate buffer (pH 7.4) using sonication. The protein concentration of the soluble fraction was determined using a BCA assay. Tyramine SULT activity was determined with cell lysates containing 100 μg total protein, supplemented with 100 μM tyramine, 100 μM PAPS (cat. no. ES019, R&D Sytems) and 1 mM pargyline (cat. no. 10007852, Cayman), a monoamine oxidase inhibitor. The assay was initiated by incubation at 30 °C for 30 min and stopped by adding ice-cold acetonitrile:methanol. SULT expression was validated using immunoblotting. SULT1D1 was not expressed in HEK 293T cells because of its incomplete sequence in UniProt. The activity was also indistinguishable from non-transfected controls. Heat-inactivated cell lysates exhibited non-detectable enzymatic activity.

Tyramine and pTOS extraction from cultured medium for LC–MS

To extract metabolites from the medium of cultured hepatocytes or bacteria, 200 μl of 1-butanol was added to 500 μl of medium. The mixture was vortexed for 1 min and then centrifuged at 4 °C for 10 min at 21,130*g*. The top layer was carefully transferred to mass spec vials for LC–MS analysis.

Mouse blood and plasma sample preparation for LC–MS

Blood from mice was collected by submandibular bleeding into lithium heparin tubes (cat. no. 365985, Becton Dickson) and immediately kept on ice. Blood was then centrifuged at 4 °C for 5 min at 2,348*g*. Plasma was transferred into new Eppendorf tubes and stored at −80 °C if not used immediately. Metabolites were then extracted by adding 150 μl of a 2:1 mixture of acetonitrile:methanol to 50 μl of serum or plasma.

CSF collection and preparation for LC–MS

Mice were anaesthetized using isoflurane (cat. no. R510-22, RWD Life Science), with a 5% concentration for induction and 2% for maintenance. Once properly anaesthetized, the mouse's head was secured onto a custom-made surgical frame in a vertical downward position to locate the cisterna magna. A sagittal incision was made along the midline of the skin, and the subcutaneous tissue and neck muscles were carefully separated to expose the cisterna magna. A 34 G needle (cat. no. 207434-10, Hamilton), connected to a Hamilton syringe (cat. no. 7643-01), was carefully inserted into the cisterna magna after piercing the atlanto-occipital membrane. CSF was slowly withdrawn from each mouse. Then, 30 μl 2:1 acetonitrile:methanol was added to 10 μl CSF to extract the metabolites in CSF.

Tyramine and pTOS measurements in the mouse brain

WT C57BL6/J 11–12-week-old male mice were injected with pTOS (50 mg kg^{-1}) or tyramine (28.7 mg kg^{-1}) or vehicle at the same molarity. Mice were anaesthetized 30 min after the administration and the brain was perfused with ice-cold PBS via cardiac perfusion. The brain was carefully dissected out and water was added at 2:1 volume-to-weight ratio (that is, 800 μl water added to 400-mg brain). After homogenization, 50 μl of the supernatant was mixed with 150 μl 2:1 acetonitrile:methanol to extract metabolites for LC–MS.

LC–MS analysis

Untargeted metabolomics measurements were performed using an Agilent 6545 Quadrupole time-of-flight LC–MS instrument. MS analysis was performed using electrospray ionization in both positive and negative modes. The dual electrospray ionization source parameters were set as follows: the gas temperature was set at 250 °C with a drying gas flow of 12 l min^{-1} and the nebulizer pressure at 20 psi; the capillary voltage was set to 3,500 V; and the fragmentor voltage was set to 100 V. Separation of metabolites was conducted using a Luna 5 μm NH_2 100 Å LC column (cat. no. 00B-4378-E0, Phenomenex) with normal phase chromatography. Mobile phases in positive mode were: buffer A, water with 0.1% formic acid; buffer B, acetonitrile with 0.1% formic acid. Mobile phases in negative mode were: buffer A, 95:5 water:acetonitrile with 0.1% ammonium hydroxide and 10 mM ammonium acetate; buffer B, acetonitrile. The LC gradient started at 100% buffer B with a flow rate of 0.7 ml min^{-1} from 0 to 2 min. The gradient was then linearly increased

to 50% buffer A and 50% buffer B at a flow rate of 0.7 ml min^{-1} from 2 to 20 min. From 20 to 25 min, the gradient was maintained at 50% buffer A and 50% buffer B at a flow rate of 0.7 ml min^{-1}.

Quantification of metabolite concentration was performed by generating a standard curve with known concentrations of each metabolite. Metabolite standards were analysed alongside the samples using the same method. A standard curve generated from the metabolite concentrations and the extracted ion intensities was used to calculate the concentrations of each metabolite.

TSE PhenoMaster metabolic studies in mice

Sixteen-week-old C57BL6/J male mice were acclimated into the TSE PhenoMaster Metabolic Cage system. In the TSE PhenoMaster cages, mice were maintained on a chow diet for the first 3 days and then fasted for 24 h followed by injection with vehicle or pTOS (50 mg kg^{-1}, intraperitoneally) and refeeding at 5:30 before the start of the night cycle, while food intake, RER, energy expenditure and locomotion were continuously monitored. Energy expenditure data were analysed with each animal's body weight as a covariate using the online CalR tool[45]. A mixture of 18:1:1 (by volume) of saline:Kolliphor EL:DMSO was used as vehicle. pTOS was dissolved in the mixture, then aliquoted and stored at −80 °C before use.

Conditioned flavour avoidance

Eight-week-old mice were habituated to restricted water access for 2 h per day (6:30 to 8:30) for 7 days. Food was available ad libitum. Training consisted of two training days. On each training day, mice had access to two burettes containing the same flavour of Kool-Aid (cherry or grape) during the fluid access period of 2 h. Immediately after, each mouse received an intraperitoneal injection of saline, pTOS (50 mg kg^{-1}) or LiCl (95 mg kg^{-1}). LiCl (cat. no. L9650, Sigma-Aldrich) was dissolved in saline and used as the positive control. The order of drug/saline exposure and paired flavours was counterbalanced on different days. Each training day was followed by a non-injection day when water was available during the 2-h fluid access period. Two days after the final training day, animals were provided with both flavours (one flavour per burette) during the 90-min fluid access period. Fluid intake was recorded for 2 h. Th pTOS or LiCl preference was calculated by dividing the consumption of pTOS or LiCl-paired flavour by the total consumption of cherry-flavoured and grape-flavoured water.

Sucrose preference test

Twelve-week-old C57BL6/J male mice were habituated with two bottles of water for 2 days. Mice were then water-deprived for 24 h and then provided with a free choice of either drinking 1% sucrose solution or double-distilled water for 2 h (6:30 to 8:30). Sucrose preference was calculated by dividing the consumption of sucrose by the total consumption of water and sucrose.

Hormone measurements

Twelve-to-fourteen-week-old DIO male mice were administered pTOS (50 mg kg, intraperitoneally) or vehicle control in the light phase (Zeitgeber time 6), with ad libitum access to food and water during the experiment. Blood was collected from mice at the 1-h and 3-h time points. The following hormones were measured with commercially available enzyme-linked immunosorbent assay kits according to the manufacturers' instructions: ghrelin (cat. no. EZRGRT-91K, Merck Millipore), leptin (cat. no. 90030, Crystal Chem), adiponectin (cat. no. 80569, Crystal Chem), insulin (cat. no. 62100, Crystal Chem), GLP-1 (cat. no. 81508, Crystal Chem) and GDF15 (cat. no. MGD150, R&D Systems).

Measurement of blood glucose levels after pTOS injection

Male C57BL/6 mice aged 8–10 weeks were fasted for 6 h from 10:00 to 16:00 and then given intraperitoneal injections of pTOS (50 mg kg^{-1}, $n = 7$) or vehicle ($n = 7$). Blood glucose levels were measured at 0, 20, 40, 60, 90 and 120 min after the injections with a glucometer.

Blood pressure measurements

Mice were anaesthetized with isoflurane and placed in the supine position with the fur removed in the chest area. Blood pressure was measured with a 1.4-F pressure sensor mounted Millar catheter (SPR-671, ADInstruments) inserted into the right carotid artery. Blood pressure was recorded with LabChart 7 Pro (ADInstruments) and annotated with the BP_annotate package in MATLAB[45,46].

Oral glucose tolerance test with pTOS injection

Male C57BL6/J mice aged 15 weeks were fasted for 4 h from 10:00 to 14:00. Mice received intraperitoneal injections of pTOS (50 mg kg^{-1}, $n = 5$) or vehicle ($n = 5$) at 13:30 and then received glucose by oral gavage (1.5 g kg^{-1}) at 14:00. Blood glucose levels were measured at 0, 20, 40, 60, 90 and 120 min after glucose oral gavage with a glucometer.

Oral lipid tolerance test with pTOS injection

Male 13-week-old C57BL6/J mice were fasted for 4 h from 9:30 am to 13:30. Mice received intraperitoneal injections of pTOS (50 mg kg^{-1}, $n = 5$) or vehicle ($n = 5$) at 13:00, and then received corn oil by oral gavage (15 µl g^{-1}) at 13:30. Blood plasma was collected at 0, 1, 2, 4, 6 and 8 h after oral gavage and triglyceride levels were measured with a colorimetric assay kit (cat. no. 10010303, Cayman).

Oral protein tolerance test with pTOS injection

Male C57BL6/J mice aged 15 weeks were fasted for 4 h from 9:30 to 13:30. Mice received intraperitoneal injections of pTOS (50 mg kg^{-1}, $n = 5$) or vehicle ($n = 5$) at 13:00, and then received ISOPURE protein powder by oral gavage (1.5 kcal kg^{-1}) at 13:30. Blood plasma was collected at 0, 0.5, 1, 2 and 4 h after oral gavage. Branched chain amino acids (that is, leucine, isoleucine and valine) were used as markers of protein intake and measured with LC–MS.

Gastric emptying assay

Male C57BL/6 mice aged 12 weeks were fasted for 12 h and then given intraperitoneal injections of pTOS (50 mg kg^{-1}, $n = 5$), exenatide (100 µg kg^{-1}, $n = 4$) or vehicle ($n = 5$). After a 30-min interval, animals received 300 µl of a phenol-red-based test meal (50 mg phenol red dissolved in 100 ml of 1.5% carboxymethylcellulose, maintained at 37 °C with gentle stirring) via oral gavage. Mice were euthanized either immediately after gavage (t = 0) or 30 min after gavage (t = 30). Stomachs were excised, homogenized in 25 ml of 0.1 N NaOH and allowed to stand for 1 h at room temperature. From the resulting mixture, 8 ml of supernatant was combined with 1 ml of 33% trichloroacetic acid, followed by centrifugation at 845*g* for 30 min at 4 °C. The clarified supernatant was then neutralized with 2 ml of 2 N NaOH and the phenol red content was quantified by measuring absorbance at 560 nm. Gastric emptying was calculated according to the following equation: gastric emptying = 100×(1-X/Y), where X represents the mean absorbance from animals euthanized at t = 30 and Y represents the mean absorbance from animals euthanized at t = 0.

TRAP2 mice

We crossed *TRAP2* mice (cat. no. 030323, The Jackson Laboratory) with *Rosa26-LSL-tdTomato* mice (cat. no. 007905, The Jackson Laboratory) to generate *TRAP2/Rosa26-LSL-tdTomato* or *TRAP2* mice. Mice were housed in a temperature-controlled environment using a 12-h light and 12-h dark cycle. Mice were individually housed at least 1 week before the study. Mice were fed a standard chow diet (19.0% protein, 6.5% fat, 2.7% crude fibre, 12.3% neutral detergent fibre, by weight, Harlan Teklad, cat. no. 2920). Water was provided ad libitum.

TRAP induction

We dissolved 4-OHT (cat. no. H6278, Sigma-Aldrich) at 20 mg ml^{-1} in ethanol by sonication at 37 °C for 15 min. The dissolved 4-OHT was then stored in aliquots at −80 °C for up to several weeks or used

immediately. Before use, 4-OHT was dissolved by shaking at 37 °C for 10 min, then sunflower seed oil and castor oil (4:1) was added for a final concentration of 10 mg ml^{-1}. After evaporating the ethanol in a vacuum (845*g*, 15 min), the final 4-OHT solution was injected intraperitoneally at 50 mg kg^{-1}. To TRAP pTOS-activated neurons, *TRAP2/Rosa26-LSL-tdTomato* 10-week-old male mice were fasted from 12:00 to 17:00, then received intraperitoneal injection of pTOS (50 mg kg^{-1}), followed by 4-OHT injection (50 mg kg^{-1}, intraperitoneally) 30 min after; 2 weeks later, mice were perfused with saline followed by 10% formalin. As controls, another group of *TRAP2/Rosa26-LSL-tdTomato* male mice received intraperitoneal injection of vehicle, followed by 4-OHT injection (50 mg kg^{-1}, intraperitoneally) 30 min after; 2 weeks later, mice were perfused. A mixture of 18:1:1 (by volume) of saline:Kolliphor EL:DMSO was used as vehicle. Coronal brain sections were cut at 30 µm and collected into five consecutive series. Sections were cover-slipped and analysed using a fluorescence microscope. The numbers of tdTomato-labelled (TRAPed) neurons were counted and quantified manually. Briefly, for each mouse brain structure analysed, anatomically defined reactive oxygen species (ROIs) were selected based on the Allen Mouse Brain Atlas. The same ROI boundaries were consistently applied across all mice and sections. To ensure consistency, a single coronal brain section per region was analysed for each mouse, selected at matched anterior-posterior coordinates based on anatomical landmarks. Three mice were included in each group.

Chemogenetic approaches

Eight-week-old Male *TRAP2* mice were anaesthetized (with 2% isoflurane) and placed in a stereotaxic instrument. Artificial eye ointment was applied to prevent corneal drying, and a heat pad was used to hold the body temperature at 37 °C. To chemogenetically inhibit pTOS-activated PVH or VMH neurons, we injected AAV8-DIO-hM4Di-mCherry (titre: 5×10^{12} GC per ml, 0.2 µl, cat. no. 44362, Addgene) into the PVH or VMH of TRAP2 mice (PVH: −0.82 mm; mediolateral: 0.25 mm; dorsoventral: −4.75 mm; VMH: −1.7 mm; mediolateral: 0.3 mm; dorsoventral: −5.6 mm), respectively. After allowing 2 weeks for virus expression, mice were housed singly before they were subjected to any studies. Mice were fasted overnight (from 17:00 to 9:00), then received saline or CNO (intraperitoneally, 3 mg kg^{-1}, cat. no. 16882, Cayman) injections. After saline or CNO injection, pre-weighed regular chow (6.5% fat; cat. no. 2020, Harlan Teklad) was put back into the cages. Food intake was monitored for 3 h. At the end of the experiments, all mice were perfused with saline followed by 10% formalin. Brain sections were collected and sectioned at 30 µm. The expression of mCherry was examined with histology; only those with accurate targeting were included in the data analyses.

cFos mapping of pTOS-activated neurons in python brains

To process python brains, we adapted the approach as previously described for in vivo fixation of the lizard brain[47]. One hour after delivery of 50 mg kg^{-1} pTOS via oral gavage, ball pythons were anaesthetized via isoflurane inhalation for 30 min. Sufficient anaesthetic depth was determined by lack of response to a physical stimulus. The thoracic cavity and rostral ~5 cm were then opened with surgical scissors to expose the heart and carotid arteries. Fine incisions were made in the ventricle and right atrium, and a perfusion needle was inserted into the ventricular incision, through the right aorta and into the left carotid artery. The needle was clamped in place with a haemostat and 50 ml of heparinized PBS (10 units per litre) was perfused using a peristaltic pump to clear blood from the brain. Brain fixation was performed by perfusion with 50 ml of 4% paraformaldehyde (PFA). The brain was then extracted using a corneoscleral punch and submerged overnight in 4% PFA at 4 °C. The brain was removed from PFA, carefully rinsed twice with PBS and then added to a 30% sucrose PBS solution and stored at 4 °C for 2 days to dehydrate the tissue. Coronal brain sections were cut at 30 µm and collected into five consecutive series. One series of the sections was blocked for 1 h in 0.3% PBS with Tween 20 with 5% normal donkey serum. To detect cFos expression, a Rabbit anti-cFos antibody (1:500 dilution, cat. no. 226008, Synaptic System) was added and incubated at 4 °C overnight on shaker. The cFos antibody recognizes the amino acid sequence 'MFSGFNADYEASSSR'. Three of the 15 amino acids in this sequence differ from those in the corresponding sequence in the python sequence. The following day, slices were rinsed with 0.1% PBS with Tween 20 for 6×10 min and then incubated with donkey anti-rabbit Alexa Fluor 488 (1:500 dilution, cat. no. A21206, Invitrogen) at room temperature for 2 h. Sections were cover-slipped and analysed using a fluorescence microscope. The numbers of cFos-labelled neurons were counted and quantified manually. The ROIs for each ball python brain structure were selected using the most reliable anatomical landmarks available from the limited existing references. For each ball python, 3–4 coronal brain sections per VMH were analysed. Four pythons were included in each group. The locations of $cFos^+$ neurons in the VMH and other brain regions were mapped onto the standard anatomical brain sections of *P. regius*[34]. Furthermore, brain sections from both the same species of red-sided garter snake[48,49] and different species with similar brain structures, such as the tree lizard *Urosaurus ornatus*[50], revealed consistent VMH locations. Within the Squamata order, the VMH is one of the brain regions having the least variation, as determined by calculating the log-transformed coefficient of variation for each brain region to assess individual differences[51].

Slice electrophysiology

Electrophysiology recordings were performed as described previously[52]. Briefly, mice were deeply anaesthetized with isoflurane and transcardially perfused with a modified ice-cold sucrose-based cutting solution (pH 7.3) containing 10 mM NaCl, 25 mM $NaHCO_3$, 195 mM sucrose, 5 mM glucose, 2.5 mM KCl, 1.25 mM NaH_2PO_4, 2 mM Na-pyruvate, 0.5 mM $CaCl_2$ and 7 mM $MgCl_2$, bubbled continuously with 95% O_2 and 5% CO_2. Mice were then decapitated and the entire brain was removed and immediately submerged in the cutting solution. Coronal brain slices (220 µm) containing the PVH or VMH were cut with a Microm HM 650V vibratome (Thermo Fisher Scientific) in oxygenated cutting solution. Slices were then incubated in oxygenated artificial CSF (126 mM NaCl, 2.5 mM KCl, 2.4 mM $CaCl_2$, 1.2 mM NaH_2PO_4, 1.2 mM $MgCl_2$, 11.1 mM glucose and 21.4 mM $NaHCO_3$, balanced with 95% O_2/5% CO_2, pH 7.4) to recover ~25 min at 32 °C and subsequently for 1 h at room temperature before recording. Slices were transferred to a recording chamber and allowed to equilibrate for at least 10 min before recording. Slices were superfused at 32 °C in oxygenated artificial CSF at a flow rate of 1.8-2 ml min^{-1}. mCherry or tdTomato-labelled neurons were visualized using epifluorescence and infrared differential interference contrast imaging on an upright microscope (Eclipse FN-1, Nikon) equipped with a movable stage (MP-285, Sutter Instrument). Patch pipettes with resistances of 3–5 MΩ were filled with intracellular solution (pH 7.3) containing 128 mM K-Gluconate, 10 mM KCl, 10 mM HEPES, 0.1 mM EGTA, 2 mM $MgCl_2$, 0.05 mM Na-GTP and 4 mM Mg-ATP. Recordings were made using a MultiClamp 700B amplifier (Axon Instrument), sampled using Digidata 1440A and analysed offline with the pClamp 10.3 software (Axon Instruments). Series resistance was monitored during the recording; values were generally less than 10 MΩ and were not compensated. The liquid junction potential was +12.5 mV and was corrected after the experiment. Data were excluded if the series resistance increased dramatically during the experiment or without overshot for action potential. Currents were amplified, filtered at 1 kHz and digitized at 20 kHz. The current-clamp mode was engaged to measure the neural firing rate and resting membrane potential at the baseline or in response to CNO (10 µM). To measure the effects of pTOS on VMH and PVH neurons, the current-clamp mode was engaged to test the neural firing rate and resting membrane potential at the baseline and after bath application of pTOS (1 µM concentration as indicated in the figures). To test if pTOS directly activated VMH neurons, VMH neurons

were pretreated with a cocktail of synaptic blockers containing 30 µM CNQX, 30 µM D-AP5 and 50 µM bicuculline to block the excitatory and inhibitory synaptic inputs in the recorded VMH neurons; pTOS-induced responses were recorded as described above.

Statistics

The minimum sample size was predetermined by the nature of the experiments. For the biochemical measurements, at least 3–4 different mice or pythons per group were used. For the behavioural measurements, 7–9 different mice per group were included. For the histology studies, the same experiment was repeated in at least three different mice or pythons. For the electrophysiological studies, at least six different neurons from three different mice were included. The data are presented as the mean ± s.e.m. or as individual data points. Statistical analyses were performed using Prism (GraphPad Software) to evaluate the normal distribution and variations within and among groups. The methods of the statistical analyses were chosen based on the design of each experiment and are indicated in the figure legends.

Reporting summary

Further information on research design is available in the Nature Portfolio Reporting Summary linked to this article.

Data availability

All data generated or analysed during this study are included in this article and its supplementary Information files. Source data are provided with this paper.

References

1. Secor, S. M. & Diamond, J. A vertebrate model of extreme physiological regulation. *Nature* **395**, 659–662 (1998).
2. Tan, Y., Martin, T. G., Harrison, B. C. & Leinwand, L. A. Utility of the burmese python as a model for studying plasticity of extreme physiological systems. *J. Muscle Res. Cell Motil.* **44**, 95–106 (2023).
3. Castoe, T. A. et al. The Burmese python genome reveals the molecular basis for extreme adaptation in snakes. *Proc. Natl Acad. Sci. USA* **110**, 20645–20650 (2013).
4. Riquelme, C. A. et al. Fatty acids identified in the Burmese python promote beneficial cardiac growth. *Science* **334**, 528–531 (2011).
5. Secor, S. M. & Diamond, J. Effects of meal size on postprandial responses in juvenile Burmese pythons (*Python molurus*). *Am. J. Physiol.* **272**, R902–R912 (1997).
6. Andrew, A. L. et al. Growth and stress response mechanisms underlying post-feeding regenerative organ growth in the Burmese python. *BMC Genomics* **18**, 338 (2017).
7. Jensen, B. & Wang, T. The elusive hypertrophy of the python heart. *Physiology* **39**, 88–97 (2024).
8. Secor, S. M. Digestive physiology of the Burmese python: broad regulation of integrated performance. *J. Exp. Biol.* **211**, 3767–3774 (2008).
9. Rindom, E. et al. Rapid stimulation of protein synthesis in digesting snakes: unveiling a novel gut-pancreas-muscle axis. *Acta Physiol.* **241**, e70006 (2025).
10. Andersen, J. B., Rourke, B. C., Caiozzo, V. J., Bennett, A. F. & Hicks, J. W. Postprandial cardiac hypertrophy in pythons. *Nature* **434**, 37–38 (2005).
11. Ott, B. D. & Secor, S. M. Adaptive regulation of digestive performance in the genus *Python*. *J. Exp. Biol.* **210**, 340–356 (2007).
12. Martin, T. G., Juarros, M. A. & Leinwand, L. A. Regression of cardiac hypertrophy in health and disease: mechanisms and therapeutic potential. *Nat. Rev. Cardiol.* **20**, 347–363 (2023).
13. Martin, T. G. & Leinwand, L. A. Molecular regulation of reversible cardiac remodeling: lessons from species with extreme physiological adaptations. *J. Exp. Biol.* **227**, jeb247445 (2024).
14. Secor, S. M. & Diamond, J. M. Evolution of Regulatory responses to feeding in snakes. *Physiol. Biochem. Zool.* **73**, 123–141 (2000).
15. Crocini, C. et al. Postprandial cardiac hypertrophy is sustained by mechanics, epigenetic, and metabolic reprogramming in pythons. *Proc. Natl Acad. Sci. USA* **121**, e2322726121 (2024).
16. Secor, S. M., Nagy, T. R., Johnston, K. E. & Tamura, T. Effect of feeding on circulating micronutrient concentrations in the Burmese python (*Python molurus*). *Comp. Biochem. Physiol. A Mol. Integr. Physiol.* **129**, 673–679 (2001).
17. Enok, S., Simonsen, L. S., Pedersen, S. V., Wang, T. & Skovgaard, N. Humoral regulation of heart rate during digestion in pythons (*Python molurus* and *Python regius*). *Am. J. Physiol.* **302**, R1176–R1183 (2012).
18. Secor, S. M. & Diamond, J. Determinants of the postfeeding metabolic response of Burmese pythons, *Python molurus*. *Physiol. Zool.* **70**, 202–212 (1997).
19. Steinberg, J. L. et al. Effects of tricyclic antidepressant treatment on tyramine-O-sulfate excretion in depressed patients. *J. Affect. Disord.* **27**, 29–34 (1993).
20. Stewart, J. W., Harrison, W., Cooper, T. B. & Quitkin, F. M. Tyramine sulfate excretion may be a better predictor of antidepressant response than monoamine oxidase activity. *Psychiatry Res.* **25**, 195–201 (1988).
21. Weinisch, P. et al. The HuMet Repository: watching human metabolism at work. *Cell Rep.* **43**, 114416 (2024).
22. Moholdt, T. et al. The effect of morning vs evening exercise training on glycaemic control and serum metabolites in overweight/obese men: a randomised trial. *Diabetologia* **64**, 2061–2076 (2021).
23. Agueusop, I., Musholt, P. B., Klaus, B., Hightower, K. & Kannt, A. Short-term variability of the human serum metabolome depending on nutritional and metabolic health status. *Sci. Rep.* **10**, 16310 (2020).
24. Voldstedlund, C. T. et al. Exercise-induced increase in muscle insulin sensitivity in men is amplified when assessed using a meal test. *Diabetologia* **67**, 1386–1398 (2024).
25. Marcobal, A., De Las Rivas, B., Landete, J. M., Tabera, L. & Muñoz, R. Tyramine and phenylethylamine biosynthesis by food bacteria. *Crit. Rev. Food Sci. Nutr.* **52**, 448–467 (2012).
26. Nowell, S. & Falany, C. N. Pharmacogenetics of human cytosolic sulfotransferases. *Oncogene* **25**, 1673–1678 (2006).
27. Ma, P. et al. Gut microbiota metabolite tyramine ameliorates high-fat diet-induced insulin resistance via increased Ca^{2+} signaling. *EMBO J.* **43**, 3466–3493 (2024).
28. Gainetdinov, R. R., Hoener, M. C. & Berry, M. D. Trace amines and their receptors. *Pharmacol. Rev.* **70**, 549–620 (2018).
29. Borowsky, B. et al. Trace amines: identification of a family of mammalian G protein-coupled receptors. *Proc. Natl Acad. Sci. USA* **98**, 8966–8971 (2001).
30. Bönisch, H. & Trendelenburg, U. in *Catecholamines I* (eds Trendelenburg, U. & Weiner, N.) 247–277 (Springer, 1988).
31. DeNardo, L. A. et al. Temporal evolution of cortical ensembles promoting remote memory retrieval. *Nat. Neurosci.* **22**, 460–469 (2019).
32. Krashes, M. J. et al. Rapid, reversible activation of AgRP neurons drives feeding behavior in mice. *J. Clin. Invest.* **121**, 1424–1428 (2011).
33. Armbruster, B. N., Li, X., Pausch, M. H., Herlitze, S. & Roth, B. L. Evolving the lock to fit the key to create a family of G protein-coupled receptors potently activated by an inert ligand. *Proc. Natl Acad. Sci. USA* **104**, 5163–5168 (2007).

34. Smeets, W. J. Distribution of dopamine immunoreactivity in the forebrain and midbrain of the snake Python regius: a study with antibodies against dopamine. *J. Comp. Neurol.* **271**, 115–129 (1988).
35. Dalile, B., Van Oudenhove, L., Vervliet, B. & Verbeke, K. The role of short-chain fatty acids in microbiota–gut–brain communication. *Nat. Rev. Gastroenterol. Hepatol.* **16**, 461–478 (2019).
36. Chiang, J. Y. L. & Ferrell, J. M. Bile acids as metabolic regulators and nutrient sensors. *Annu. Rev. Nutr.* **39**, 175–200 (2019).
37. Collins, S. L., Stine, J. G., Bisanz, J. E., Okafor, C. D. & Patterson, A. D. Bile acids and the gut microbiota: metabolic interactions and impacts on disease. *Nat. Rev. Microbiol.* **21**, 236–247 (2023).
38. Tran, L. T. et al. Hypothalamic control of energy expenditure and thermogenesis. *Exp. Mol. Med.* **54**, 358–369 (2022).
39. Joëls, M., Karst, H. & Sarabdjitsingh, R. A. The stressed brain of humans and rodents. *Acta Physiol.* **223**, e13066 (2018).
40. Calvete, J. J. et al. The disulfide bridge pattern of snake venom disintegrins, flavoridin and echistatin. *FEBS Lett.* **309**, 316–320 (1992).
41. Calvete, J. J. in *Integrin-Ligand Interaction* (eds Eble, J. A. & Kühn, K) 157–173 (Springer, 1997).
42. Acharya, K. R., Sturrock, E. D., Riordan, J. F. & Ehlers, M. R. W. Ace revisited: a new target for structure-based drug design. *Nat. Rev. Drug Discov.* **2**, 891–902 (2003).
43. Eng, J., Kleinman, W. A., Singh, L., Singh, G. & Raufman, J. P. Isolation and characterization of exendin-4, an exendin-3 analogue, from *Heloderma suspectum* venom. Further evidence for an exendin receptor on dispersed acini from guinea pig pancreas. *J. Biol. Chem.* **267**, 7402–7405 (1992).
44. Cheng, A. G. et al. Design, construction, and in vivo augmentation of a complex gut microbiome. *Cell* **185**, 3617–3636 (2022).
45. Mina, A. I. et al. CalR: a web-based analysis tool for indirect calorimetry experiments. *Cell Metab.* **28**, 656–666 (2018).
46. Laurin, A. BP_annotate. *MATLAB Central File Exchange* www.mathworks.com/matlabcentral/fileexchange/60172-bp_annotate (2025).
47. Hoops, D. A perfusion protocol for lizards, including a method for brain removal. *MethodsX* **2**, 165–173 (2015).
48. Krohmer, R. W., Boyle, M. H., Lutterschmidt, D. I. & Mason, R. T. Seasonal aromatase activity in the brain of the male red-sided garter snake. *Horm. Behav.* **58**, 485–492 (2010).
49. Martinez-Marcos, A., Ubeda-Bañon, I., Lanuza, E. & Halpern, M. Efferent connections of the 'olfactostriatum': a specialized vomeronasal structure within the basal ganglia of snakes. *J. Chem. Neuroanat.* **29**, 217–226 (2005).
50. Kabelik, D., Crombie, T. & Moore, M. C. Aggression frequency and intensity, independent of testosterone levels, relate to neural activation within the dorsolateral subdivision of the ventromedial hypothalamus in the tree lizard Urosaurus ornatus. *Horm. Behav.* **54**, 18–27 (2008).
51. Hoops, D. et al. A fully segmented 3D anatomical atlas of a lizard brain. *Brain Struct. Funct.* **226**, 1727–1741 (2021).
52. Scanferla, A. in *The Origin and Early Evolutionary History of Snakes* (eds Gower, D. J. & Zaher, H.) 294–315 (Cambridge Univ. Press, 2022).

Acknowledgements

We thank members of the Long laboratory for discussions. We thank B. Gallardo for assistance in laboratory operations. We thank J. Van Vranken for assistance with the multiplex proteomics at Harvard Medical School. We thank H. Lavach in the BioFrontiers Institute at the University of Colorado for the expert help with python microbiome studies. This work was supported by the US National Institutes of Health (grant nos. R01GM029090 to L.A.L., R01DK138518 to Y.X., R01DK105203 and R01DK124265 to J.Z.L., K99DK141966 to S.X., K99AR081618 to M.Z., F32HD112123 to M.W., F32HL170637 to T.G.M., F32DK138685 to X.F. and T32GM142607 to M.P.M.), the Wu Tsai Human Performance Alliance (research grant to J.Z.L., postdoctoral fellowship to S.X.), the Stanford Diabetes Research Center (grant no. P30DK116074 to J.Z.L.), the Phil and Penny Knight Initiative for Brain Resilience at the Wu Tsai Neurosciences Institute (research grant to J.Z.L.), the Ono Pharma Foundation (research grant to J.Z.L.), the Weill Cancer Hub West (research grant to J.Z.L.), the Leducq Foundation (grant no. 21CVD02 to L.A.L.), the American Heart Association (grant nos. 24POST1200064 to S.X. and 24POST1196199 to W.W.) and the Stanford University Medical Scientist Training Program (grant no. T32-GM007365 to S.D.T.). The clinical trial of the Moholdt Study was supported by the Novo Nordisk Foundation (grant no. NNF14OC0011493 to J.A.H.) and The Liaison Committee for Education, Research and Innovation in Central Norway (no. 2016/29014 to T.M.).

Author contributions

Conceptualization: S.X. and J.Z.L. Investigation: S.X., M.W., T.G.M., B.S. X.F., X.L., Y.Y., S.F., S.D.T., J.F.G., G.L.M., M.P.M., J.H.H., V.L.L., A.L.M., Mingming Zhao, W.Q., S.C.R., Meng Zhao, J.S., W.W., T.M. and C.T.V. Resources: J.A.H., E.A.R., X.C., K.J.S., D.B., L.A.L., Y.X. and J.Z.L. Writing—original draft: S.X. and J.Z.L. Writing—Reviewing & Editing: S.X. M.W., T.G.M., L.A.L., Y.X. and J.Z.L. Supervision and funding acquisition: L.A.L., Y.X. and J.Z.L.

Competing interests

A provisional patent application has been filed by Stanford University on *para*-tyramine-O-sulphate for the treatment of cardiometabolic diseases. J.Z.L. and S.X. are listed inventors. J.Z.L. and K.J.S. are cofounders, equity holders and advisers to Merrifield Therapeutics. J.Z.L. is a cofounder, equity holder and adviser to Arkana Therapeutics and an adviser to Metabolize Inc. The other authors declare no competing interests.

Additional information

Extended data is available for this paper at https://doi.org/10.1038/s42255-026-01485-0.

Supplementary information The online version contains supplementary material available at https://doi.org/10.1038/s42255-026-01485-0.

Correspondence and requests for materials should be addressed to Leslie A. Leinwand, Yong Xu or Jonathan Z. Long.

Peer review information *Nature Metabolism* thanks Rachel Carmody, Daniela Cota, Stephen Secor and the other, anonymous, reviewer(s) for their contribution to the peer review of this work. Primary Handling Editor: Christoph Schmitt, in collaboration with the *Nature Metabolism* editorial team.

[1]Department of Pathology, Stanford University School of Medicine, Stanford, CA, USA. [2]Sarafan ChEM-H, Stanford University, Stanford, CA, USA. [3]Wu Tsai Human Performance Alliance, Stanford University, Stanford, CA, USA. [4]USDA/ARS Children's Nutrition Research Center, Department of Pediatrics, Baylor College of Medicine, Houston, TX, USA. [5]Department of Molecular, Cellular and Developmental Biology, University of Colorado, Boulder, CO, USA. [6]BioFrontiers Institute, University of Colorado, Boulder, CO, USA. [7]School of Biochemistry and Immunology, Trinity Biomedical Sciences Institute, Trinity College Dublin, Dublin, Ireland. [8]Department of Biology, Stanford University, Stanford, CA, USA. [9]Department of Structural Biology, Stanford University School of Medicine, Stanford, CA, USA. [10]Department of Chemical and Systems Biology, Stanford University School of Medicine, Stanford, CA, USA. [11]Department of Biochemistry, University of Colorado, Boulder, CO, USA. [12]Department of Pediatrics, Stanford University School of Medicine, Stanford, CA, USA. [13]Cardiovascular Institute, Stanford University School of Medicine, Stanford, CA, USA. [14]Stanford Diabetes Research Center, Stanford University School of Medicine, Stanford, CA, USA. [15]Department of Animal Science, University of California, Davis, CA, USA. [16]Department of Biochemistry, University of Wisconsin-Madison, Madison, WI, USA. [17]Department of Circulation and Medical Imaging, Norwegian University of Science and Technology, Trondheim, Norway. [18]Women's Clinic, St Olavs Hospital, Trondheim, Norway. [19]Exercise & Nutrition Research Program, Mary MacKillop Institute for Health Research, Australian Catholic University, Fitzroy, Victoria, Australia. [20]The August Krogh Section for Molecular Physiology, Department of Nutrition, Exercise and Sports, University of Copenhagen, Copenhagen, Denmark. [21]The Phil and Penny Knight Initiative for Brain Resilience at the Wu Tsai Neurosciences Institute, Stanford University, Stanford, CA, USA. [22]Present address: Department of Psychiatry and Behavioral Neurosciences, University of South Florida, Tampa, FL, USA. [23]These authors contributed equally: Shuke Xiao, Mengjie Wang, Thomas G. Martin. ✉e-mail: leslie.leinwand@colorado.edu; yongx@bcm.edu; jzlong@stanford.edu

https://doi.org/10.1038/s42255-026-01485-0

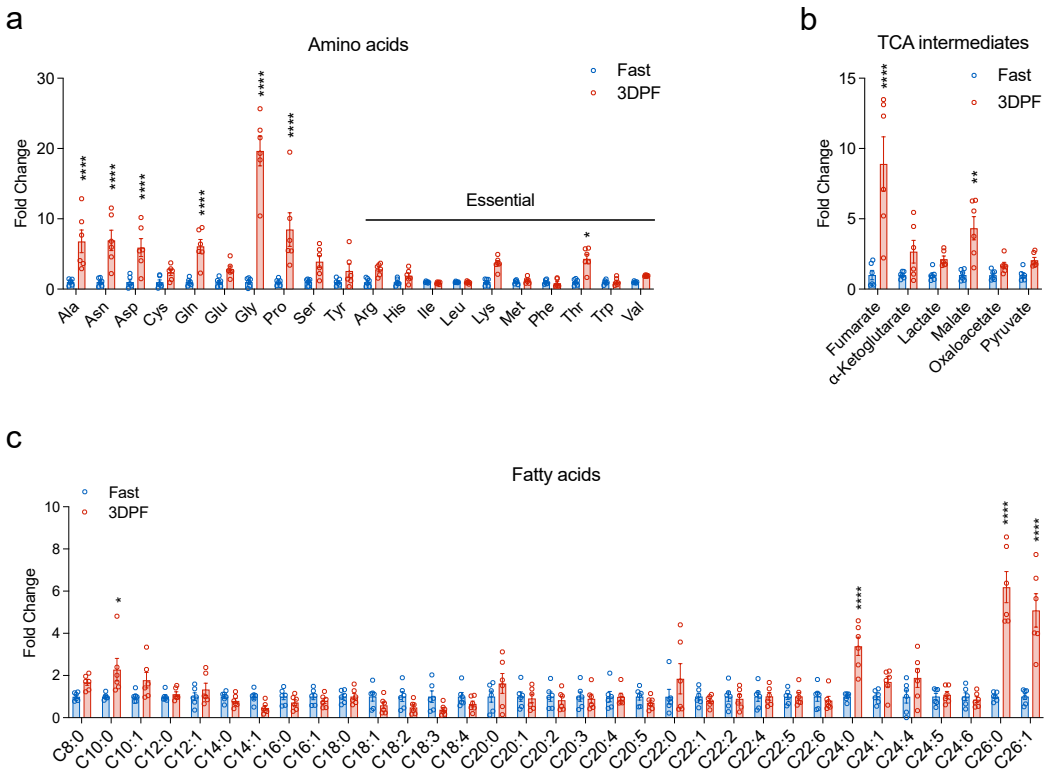

Extended Data Fig. 1 | Additional characterization of postprandial python metabolites. (**a**) Plasma levels of amino acids in 3DPF Burmese pythons compared to Fasted pythons. (**b**) Plasma levels of TCA intermediates in 3DPF Burmese pythons compared to Fasted pythons. (**c**) Plasma levels of free fatty acids in 3DPF Burmese pythons compared to Fasted pythons. Data are shown as mean ± SEM. P values were calculated using two-way ANOVA followed by Turkey's multiple comparisons test. * $P < 0.05$. ** $P < 0.01$, **** $P < 0.0001$. Exact P values are: (**a**) Ala, $P < 0.0001$, Asn, $P < 0.0001$, Asp, $P < 0.0001$, Gln, $P < 0.0001$, Gly, $P < 0.0001$, Pro, $P < 0.0001$, Thr, $P = 0.029$; (**b**) Fumarate, $P < 0.0001$, Malate, $P = 0.005$; (**c**) C10:0, $P = 0.022$, C24:0, $P < 0.0001$, C26:0, $P < 0.0001$, C26:1, $P < 0.0001$.

https://doi.org/10.1038/s42255-026-01485-0

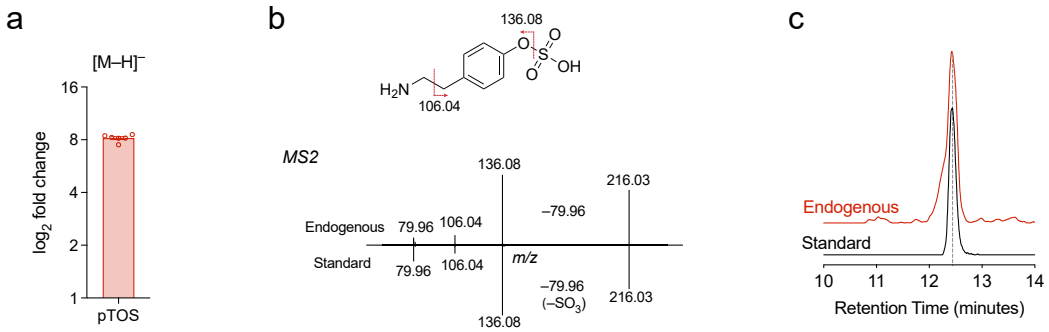

Extended Data Fig. 2 | Additional characterization of pTOS. (**a**) Detection and relative quantification of pTOS in negative ionization mode. (**b**) Tandem mass spectrometry fragmentation from endogenous m/z = 216.0331 (left, up) and synthesized pTOS standard (left, down), and the chemical structural of pTOS (right). (**c**) Co-elution of the endogenous peak and synthesized pTOS standard. Data are shown as mean ± SEM.

https://doi.org/10.1038/s42255-026-01485-0

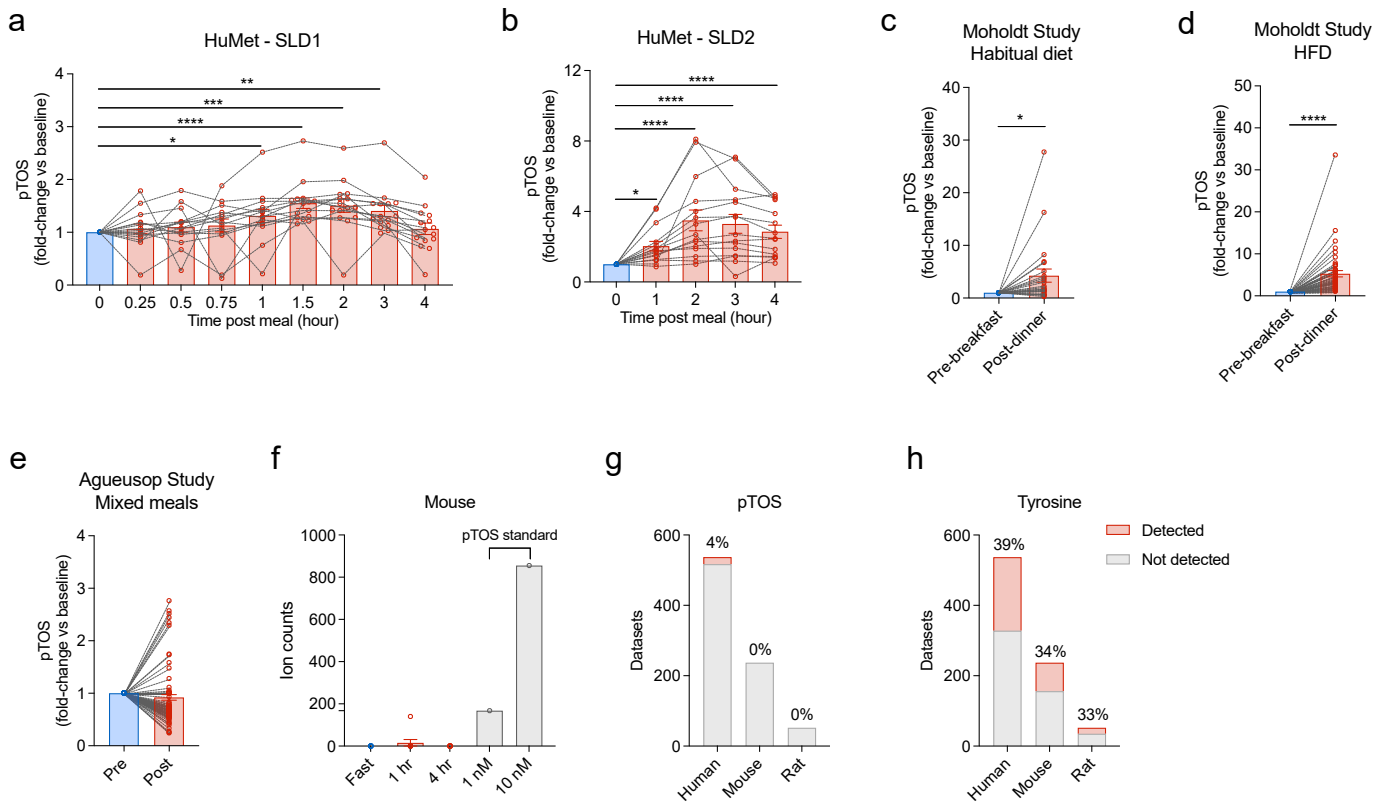

Extended Data Fig. 3 | Plasma pTOS levels in mouse, human, and rat. (**a, b**) Relative changes of pTOS levels in human plasma with two additional standardized liquid diet (SLD) meals in the 'HuMet' study (n = 15 human subjects). (**c, d**) Relative levels of pTOS before breakfast and after dinner with habitual diet (**c**) or high-fat diet (**d**) in the 'Moholdt' study (n = 24 human subjects). (**e**) Relative levels of pTOS before and 1 hr after the mixed meal test in the 'Agueusop' study (n = 90 human subjects). (**f**) Integrated ion counts of pTOS in mouse plasma after a 16-hour fast and following 1 or 4 hours of refeeding. One out of 27 samples yield a non-zero ion count. (**g**) A survey of the NIH Metabolomics Workbench (accessed 31 July 2025) showed that p-tyramine-O-sulfate (pTOS) is reported in human blood datasets but not in mouse or rat blood. (**h**) The same survey in (**g**) showed that tyrosine is roughly equally reported in human, mouse, and rat blood. In (**g, h**), detection frequency was calculated as the proportion of blood studies in which the analyte was reported. Data in (**a-e**) are shown as mean ± SEM. P values were calculated with Repeated Measures One-Way ANOVA followed by Dunnett's multiple comparisons test. *P < 0.05, **P < 0.01, ***P < 0.001, ****P < 0.0001. Exact P values are (**a**) 0 vs 1, P = 0.0371, 0 vs 1.5, P < 0.0001, 0 vs 2, P = 0.0001, 0 vs 3, P = 0.0029; (**b**) 0 vs 1, P = 0.0329, 0 vs 2, P < 0.0001, 0 vs 3, P < 0.0001, 0 vs 4, P < 0.0001; (**c**) P = 0.016; (**d**) P < 0.0001.

https://doi.org/10.1038/s42255-026-01485-0

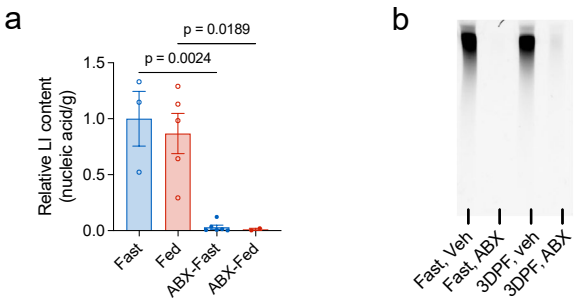

Extended Data Fig. 4 | Additional effect of antibiotics (ABX) treatment. (**a**) Relative quantities of DNA from large intestinal contents in fasted and 3DPF pythons with or without ABX treatment, normalized to the average DNA content of fasted, vehicle-treated pythons. Data are mean ± SEM. P values were calculated with two-way ANOVA with Tukey's post-hoc test. N = 3 for vehicle fast (Fast), n = 6 for ABX fast (ABX-Fast), n = 5 for vehicle 3DPF (Fed), n = 2 for ABX 3DPF (ABX-Fed). (**b**) Representative gel image showing DNA content from large intestinal contents in fasted and 3DPF pythons with or without ABX treatment.

https://doi.org/10.1038/s42255-026-01485-0

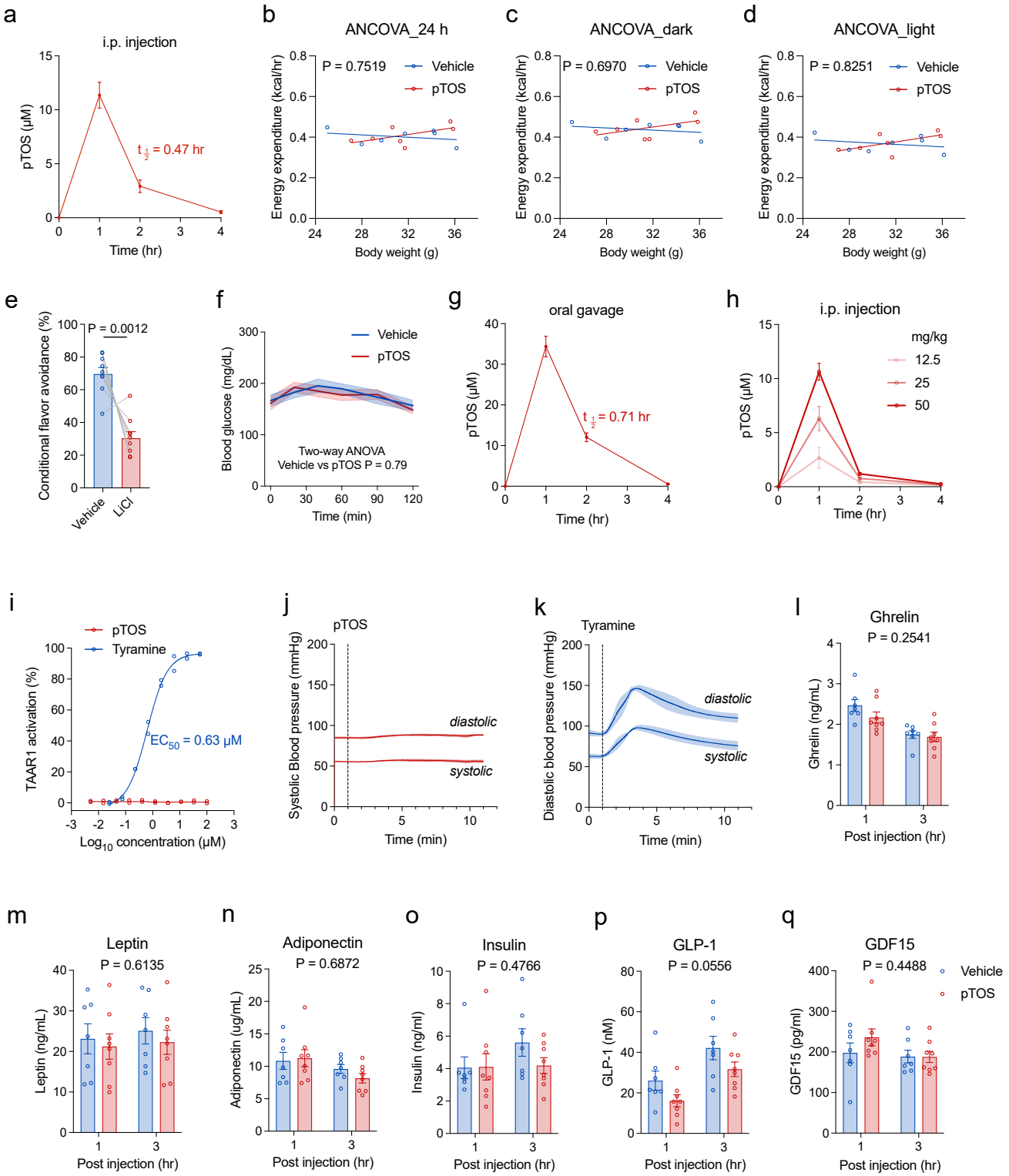

Extended Data Fig. 5 | Additional characterization of pTOS administration to mice. (**a**) Plasma levels of pTOS in C57BL6/J male mice (11-12 weeks old) post pTOS administration (50 mg/kg, i.p., n = 5). Half-life ($t_{1/2}$) was calculated with a one phase exponential decay model ($R^2 = 0.95$). (**b-d**) No change in energy expenditure with pTOS administration (50 mg/kg, i.p.) using body mass as a covariate. ANCOVA, analysis of covariance. (**e**) Conditioned flavor avoidance ratio in paired solution for male mice treated with LiCl (95 mg/kg, i.p.) or vehicle control. (n = 9/group). (**f**) Plasma glucose levels in C57BL6/J male mice (11-12 weeks old) post pTOS administration (50 mg/kg, i.p., n = 5). (**g**) Plasma levels of pTOS in C57BL6/J male mice (11-12 weeks old) post pTOS administration (50 mg/kg, p.o., n = 5). Half-life ($t_{1/2}$) was calculated with a one phase exponential decay model ($R^2 = 0.95$). (**h**) Plasma levels of pTOS in C57BL6/J male mice (14 weeks old) post pTOS administration at doses indicated (i.p., n = 5 per group). (**i**) Human TAAR1 activation utilizing a cAMP-based cellular assay. (n = 2/condition). (**j, k**) Blood pressures measured with the pressure sensor inserted into the right carotid artery of C57BL6/J male mice (10-12 weeks old) with pTOS (**j**, 50 mg/kg, i.p., n = 4), or tyramine (k, 50 mg/kg, i.p., n = 3). Dash line indicates the time of injections. (**l-q**) Plasma levels of indicated hormones in male C57BL6/J DIO mice (12-14 weeks old) at 1 hour or 3 hours after pTOS administration (50 mg/kg, i.p., n = 8) or vehicle control (n = 7). Data are shown as mean ± SEM. P values were calculated with ANCOVA (**b-d**), two-tailed paired t test (**e**), two-way ANOVA (**f**, **l-q**). Exact P values are provided in the figure.

https://doi.org/10.1038/s42255-026-01485-0

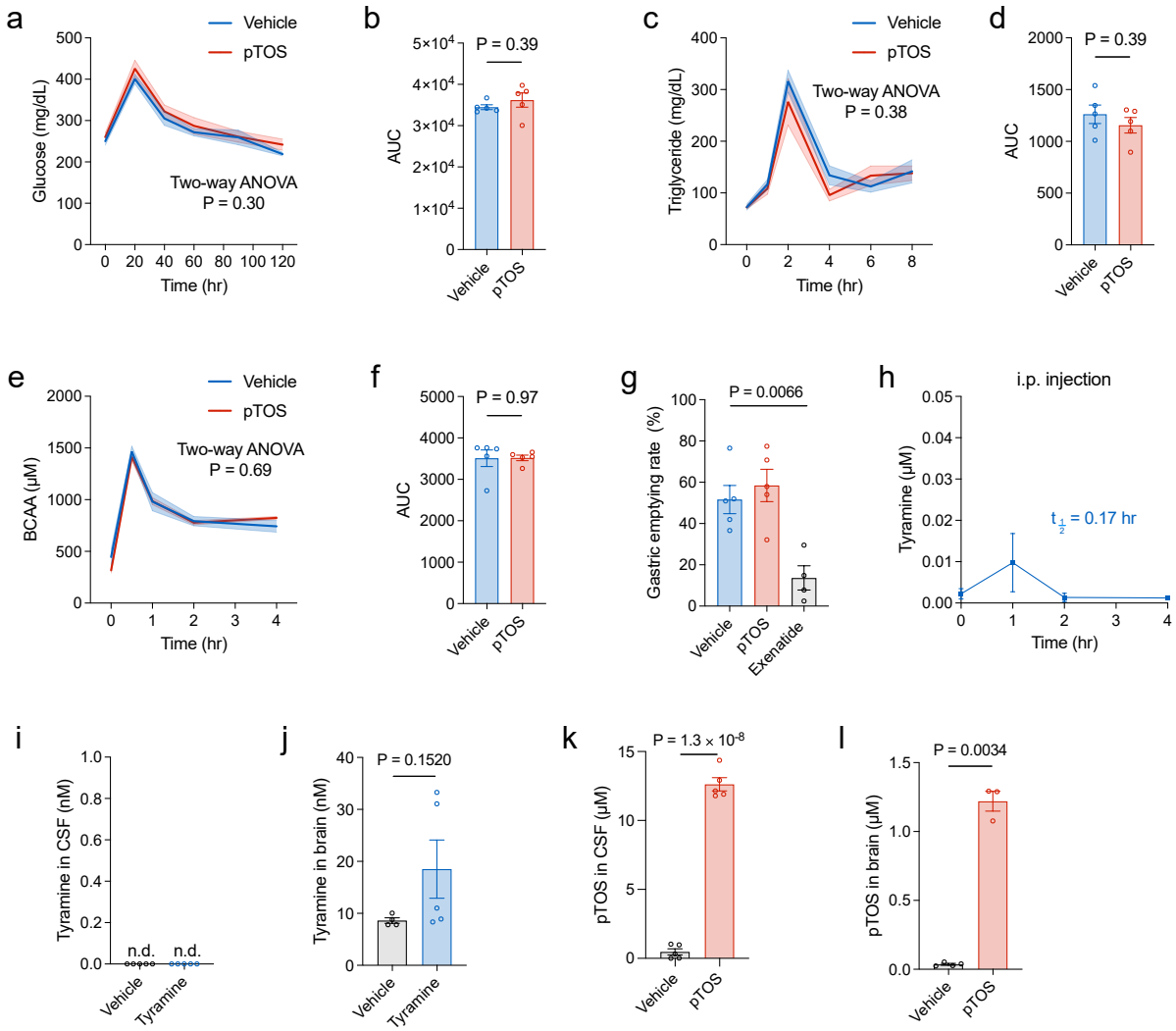

Extended Data Fig. 6 | Additional characterization of pTOS administration to mice. (**a**) Plasma glucose levels in male C57BL6/J mice (15 weeks old) during oral glucose tolerance test followed by ip injections of pTOS (50 mg/kg, n = 5), or vehicle (n = 5). (**b**) Area-under-curve (AUC) of glucose levels in (**a**). (**c**) Plasma triglyceride levels in male C57BL6/J mice (13 weeks old) during oral lipid tolerance test followed by ip injections of pTOS (50 mg/kg, n = 5), or vehicle (n = 5). (**d**) AUC of triglyceride levels in (**c**). (**e**) Plasma branched chain amino acid (BCAA) levels in male C57BL6/J mice (15 weeks old) during oral protein tolerance test followed by ip injections of pTOS (50 mg/kg, n = 5), or vehicle (n = 5). (**f**) Area-under-curve (AUC) of BCAA levels in (**e**). (**g**) Gastric emptying rate in 12-week-old male C57BL/6 mice injected (i.p.) with vehicle (n = 5), pTOS (50 mg/kg, n = 5), or exenatide (100 μg/kg, n = 4). (**h**) Plasma levels of tyramine in C57BL/6J male mice (11-12 weeks old) post tyramine administration (28.7 mg/kg, i.p., n = 4), a dose equimolar to 50 mg/kg of pTOS. (**i-l**) Tyramine and pTOS levels in CSF (**i**, **k**) or the brain lysates (**j**, **l**) 30 min after tyramine (28.7 mg/kg, i.p.) or pTOS (50 mg/kg, i.p.) injections at equimolar doses. 'n.d.', not detected. In (**i**) and (**k**), n = 5/group. In (j) and (l), n = 4 for vehicle, n = 5 for tyramine, n = 3 for pTOS. Data are shown as mean ± SEM. P values were calculated with two-way ANOVA (**a**, **c**, **e**), two-tailed t tests (**b**, **d**, **f**, **j**, **k**, **l**), one-way ANOVA followed by Šídák's multiple comparisons test (**g**). Exact P values are provided in the figure.

https://doi.org/10.1038/s42255-026-01485-0

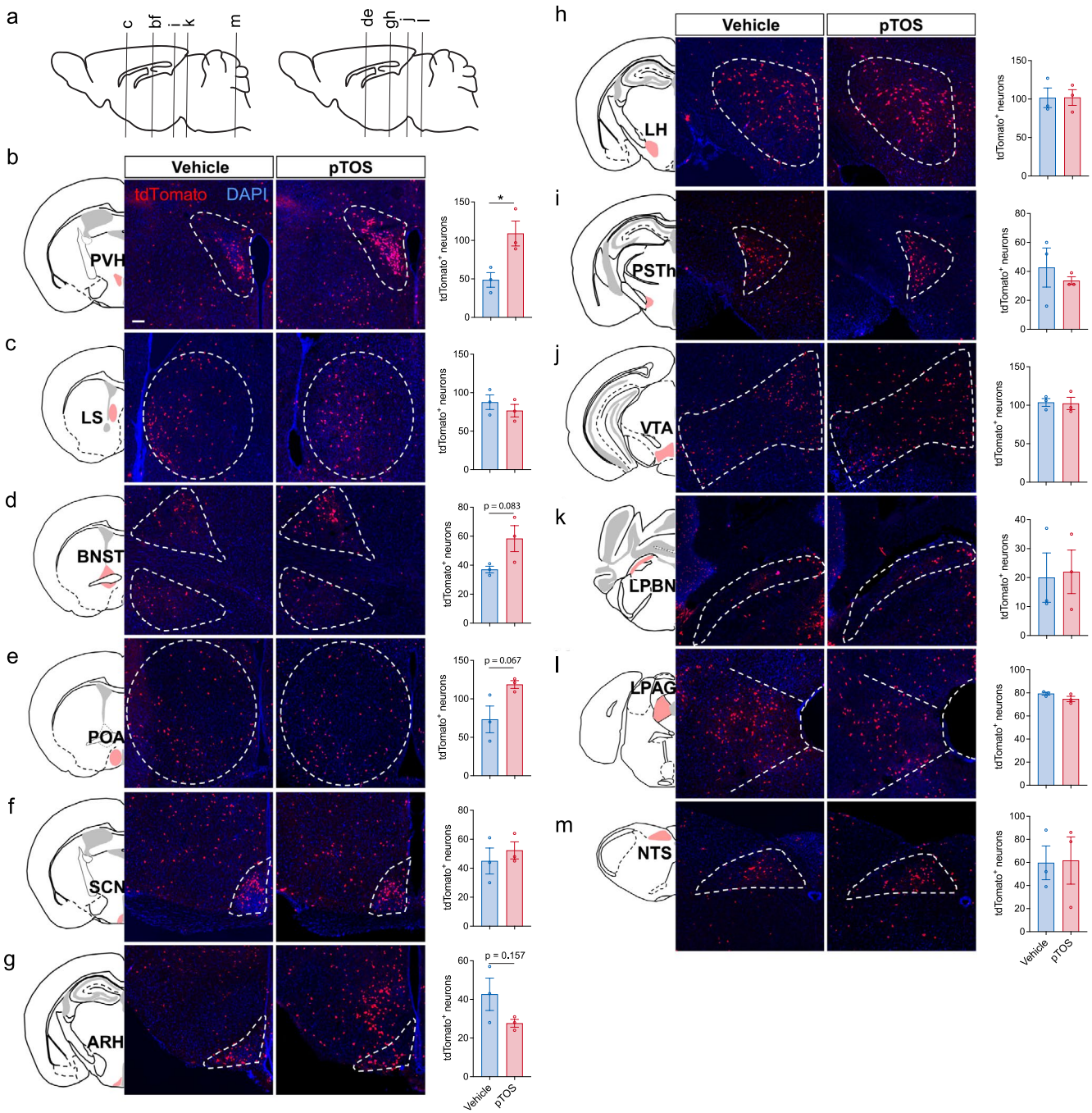

Extended Data Fig. 7 | Mapping of pTOS-activated neurons in the mouse brain. (**a**) Schematic of locations for the indicated coronal sections across the mouse brain. (**b**-**m**) Representative images and quantifications of pTOS-activated neurons in the brain regions as indicated in male *TRAP2/Rosa26-LSL-tdTomato* mice (10 weeks old, n = 3). ARH, arcuate nucleus of the hypothalamus; BNST, bed nucleus of the stria terminalis; LH, lateral hypothalamus; LPAG, lateral periaqueductal gray; LPBN, lateral parabrachial nucleus; LS, lateral septum; NTS, nucleus of the solitary tract; POA, preoptic area; PSTh, posterior subthalamic nucleus; PVH, paraventricular nucleus of the hypothalamus; SCN, suprachiasmatic nucleus; VTA, ventral tegmental area. Scale bars, 100 µm. Data are shown as mean ± SEM. P values were calculated by two-tailed t-tests. Exact P values are: (b) P = 0.0324.

https://doi.org/10.1038/s42255-026-01485-0

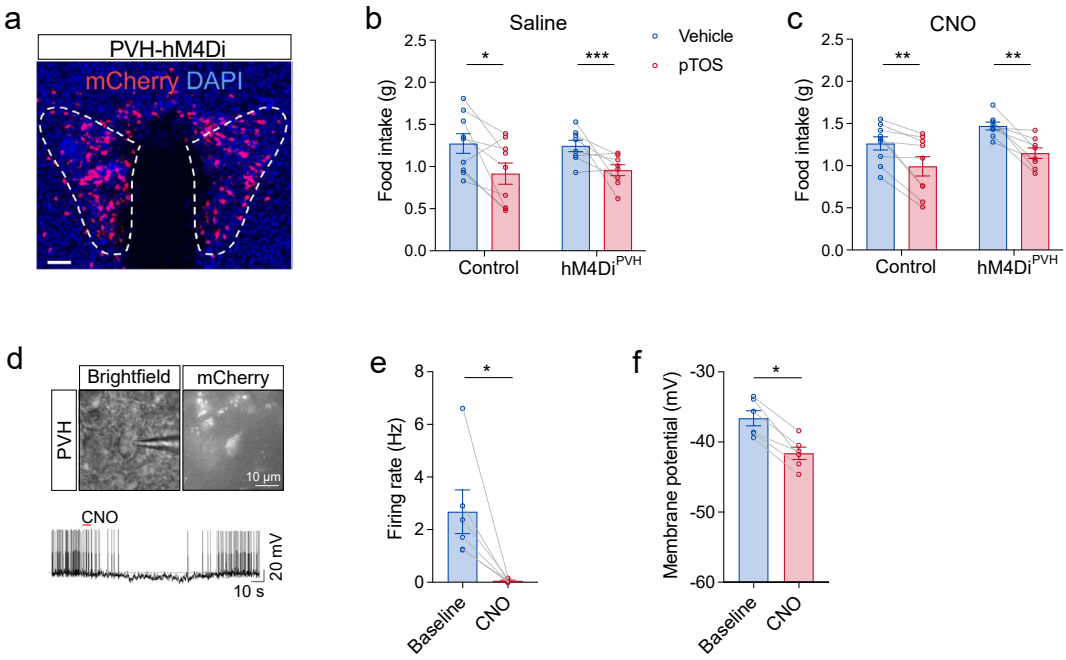

Extended Data Fig. 8 | PVH neurons do not mediate the anorexigenic effects of pTOS. (**a**) Representative image of hM4Di-mCherry expression in the PVH of male hM4Di^{PVH} mice, experiment repeated 7 times with similar results obtained. (**b**, **c**) Three-hour food intake in control or hM4Di^{PVH} mice pretreated with saline (**b**) or CNO (**c**), followed with pTOS (50 mg/kg, i.p.) or vehicle administration (n = 8-9/group, 13-16 weeks old). Vertical black bars indicate the difference in food intake between vehicle- and pTOS-treated mice. (**d**-**f**) Representative image for electrophysiological recordings (**d**, top) and representative action potential traces (**d**, bottom) and quantitation of firing rate (**e**) and resting membrane potential (**f**) of hM4Di^{PVH} neurons in response to CNO (10 µM, n = 6 neurons). Data are shown as mean ± SEM. P values were calculated using one-sided paired t-test (**b**, **c**), two-tailed Wilcoxon tests (**e**, **f**). *P < 0.05, **P < 0.01, ***P < 0.001. Exact P values are: (**b**) Control: P = 0.0153, hM4Di^{PVH} P = 0.0002; (**c**) Control: P = 0.003, hM4Di^{PVH} P = 0.001; (**e**) P = 0.0312; (f) P = 0.0312.

https://doi.org/10.1038/s42255-026-01485-0

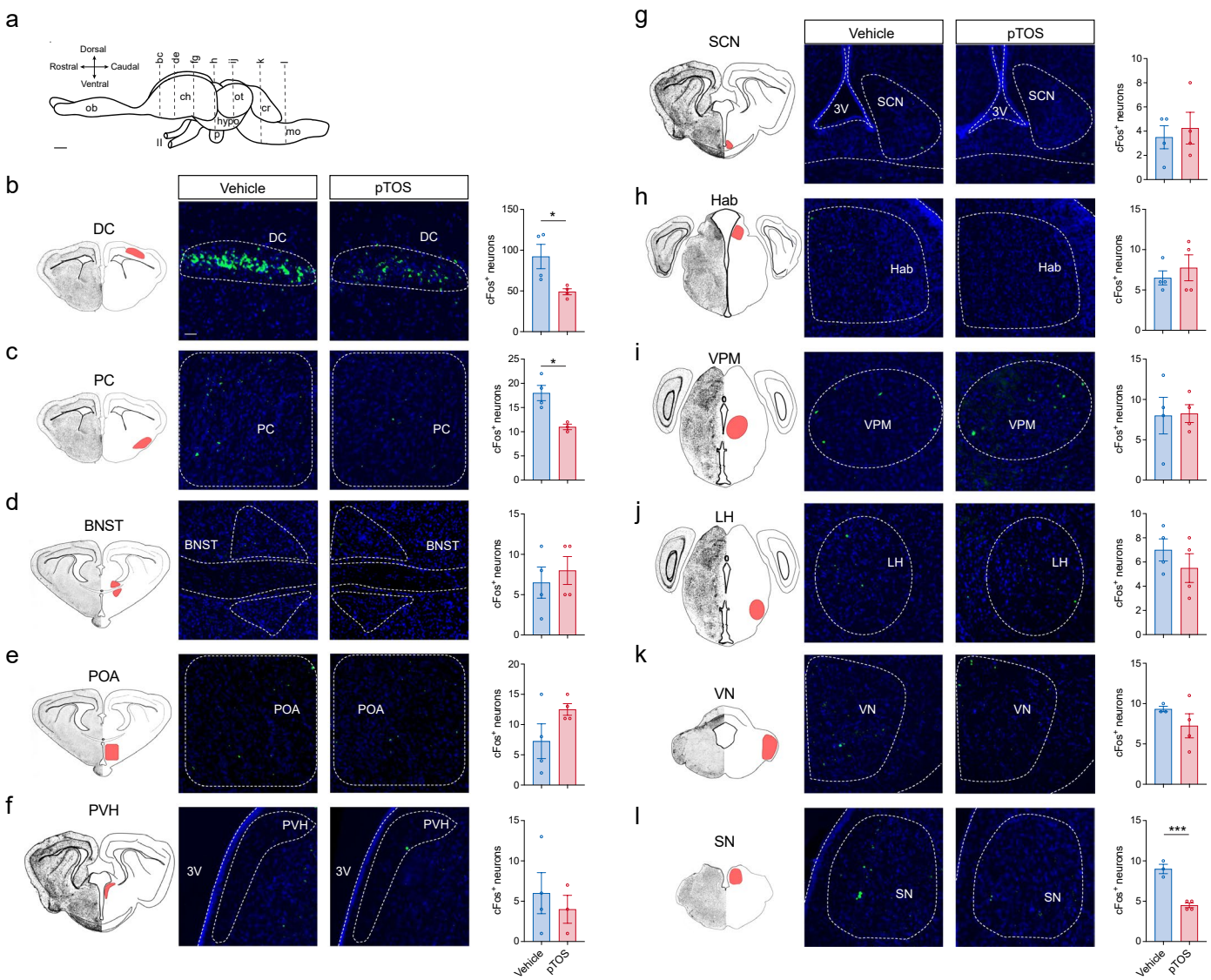

Extended Data Fig. 9 | cFos mapping of pTOS-activated neurons in the python brain. (**a**) Schematic of locations for the indicated coronal sections across the python brain (adapted from ref. 52). (**b-l**) Anatomical location (left), representative images (middle), and quantifications (right) of cFos immunofluorescence in the indicated brain regions in ball pythons after administration of pTOS (50 mg/kg, p.o.). BNST, bed nucleus of the stria terminalis; DC, dorsal cortex; Hab, habenular nucleus; LH, lateral hypothalamus; Ob, olfactory bulb; POA, preoptic area; PC, piriform cortex; PVH, periventricular nucleus of hypothalamus; SCN, suprachiasmatic nucleus; SN, spinal trigeminal nucleus; VN, vestibular nucleus; VPM, ventral posteromedial nucleus. Scale bars, 100 µm. Data are shown as mean ± SEM. In (**b**, **d-j**), n = 4/group. In (**c**), n = 4 for vehicle, n = 3 for pTOS. In (**k, l**), n = 3 for vehicle, n = 4 for pTOS. P values were calculated by two-tailed t-tests. *P < 0.05, **P < 0.01, ***P < 0.001. ****P < 0.0001. Exact P values are: (**b**) P = 0.0304; (**c**) P = 0.0152; (**n**) P = 0.0006.